



HAL
open science

Duplication of NRAMP3 gene in poplars generated two homologous transporters with distinct functions

Mathieu Pottier, van Anh Le Thi, Catherine Primard-Brisset, Jessica Marion, Michele Bianchi, Cindy Victor, Annabelle Déjardin, Gilles Pilate, Sebastien Thomine

► To cite this version:

Mathieu Pottier, van Anh Le Thi, Catherine Primard-Brisset, Jessica Marion, Michele Bianchi, et al.. Duplication of NRAMP3 gene in poplars generated two homologous transporters with distinct functions. *Molecular Biology and Evolution*, 2022, *BioRxiv*, 39 (6), pp.msac129. 10.1093/molbev/msac129 . hal-03528379

HAL Id: hal-03528379

<https://hal.inrae.fr/hal-03528379>

Submitted on 22 Nov 2022

HAL is a multi-disciplinary open access archive for the deposit and dissemination of scientific research documents, whether they are published or not. The documents may come from teaching and research institutions in France or abroad, or from public or private research centers.

L'archive ouverte pluridisciplinaire **HAL**, est destinée au dépôt et à la diffusion de documents scientifiques de niveau recherche, publiés ou non, émanant des établissements d'enseignement et de recherche français ou étrangers, des laboratoires publics ou privés.



Distributed under a Creative Commons Attribution - NonCommercial - NoDerivatives 4.0 International License

Duplication of *NRAMP3* Gene in Poplars Generated Two Homologous Transporters with Distinct Functions

Mathieu Pottier ^{†,1} Van Anh Le Thi,^{†,1} Catherine Primard-Brisset,¹ Jessica Marion,¹ Michele Wolf Bianchi ¹ Cindy Victor,¹ Annabelle Déjardin ² Gilles Pilate ² and Sébastien Thomine ^{*},¹

¹Université Paris-Saclay, CEA, CNRS, Institute for Integrative Biology of the Cell (I2BC), 91198, Gif-sur-Yvette, France

²INRAE, ONF, BioForA, F-45075, Orléans, France

[†]Present address: Institute for Molecular Physiology, Heinrich-Heine-University Düsseldorf, Düsseldorf 40225, Germany

^{*}Present address: Graduate University of Science and Technology (GUST), Vietnam Academy of Science and Technology (VAST), 18 Hoang Quoc Viet, Cau Giay, Hanoi 10000, Vietnam

***Corresponding author:** E-mail: sebastien.thomine@i2bc.paris-saclay.fr

Associate editor: Michael Pu

Abstract

Transition metals are essential for a wealth of metabolic reactions, but their concentrations need to be tightly controlled across cells and cell compartments, as metal excess or imbalance has deleterious effects. Metal homeostasis is achieved by a combination of metal transport across membranes and metal binding to a variety of molecules. Gene duplication is a key process in evolution, as the emergence of advantageous mutations on one of the copies can confer a new function. Here, we report that the poplar genome contains two paralogues encoding *NRAMP3* metal transporters localized in tandem. All *Populus* species analyzed had two copies of *NRAMP3*, whereas only one could be identified in *Salix* species indicating that duplication occurred when the two genera separated. Both copies are under purifying selection and encode functional transporters, as shown by expression in the yeast heterologous expression system. However, genetic complementation revealed that only one of the paralogues has retained the original function in the release of metals stored in the vacuole previously characterized in *Arabidopsis thaliana*. Confocal imaging showed that the other copy has acquired a distinct localization to the Trans-Golgi Network (TGN). Expression in poplar suggested that the copy of *NRAMP3* localized on the TGN has a novel function in the control of cell-to-cell transport of manganese. This work provides a clear case of neofunctionalization through a change in the subcellular localization of a metal transporter as well as evidence for the involvement of the secretory pathway in the cell-to-cell transport of manganese.

Key words: manganese, metal, recycling, Trans-Golgi Network, vacuole, *Arabidopsis*, *Salix*, *Populus*, selective pressure, evolution, apoplasmic transport, symplasmic transport, nutrition, micronutrient.

Introduction

Several transition metals are essential cofactors for a wealth of metabolic reactions in all living organisms. Iron (Fe) and copper (Cu) are, for example, needed in large amounts for the respiratory electron transfer chains and ATP production in bacteria and mitochondria. Transition metals are also important for DNA synthesis, proteolysis, and the control of reactive oxygen species. Photosynthetic organisms have an additional specific requirement for manganese (Mn) for light energy conversion and water-splitting (Shen 2015). Although they are essential, transition metal concentrations need to be tightly controlled across cells and cell compartments, as excess or imbalance between different metals has deleterious effects. Metal homeostasis is achieved by a combination of metal transport across membranes and metal binding to a variety of molecules, including proteins, small peptides, amino acids, organic acids, and specialized metabolites,

such as phytochelatins or nicotianamine in plants (Seregin and Kozhevnikova 2021).

Many families of transporters are implicated in the maintenance of metal homeostasis, either for metal uptake, distribution of metals to organs within organisms and to organelles within a cell, or for removal and sequestration of excess metal. For example, in *Arabidopsis thaliana*, Mn is taken up by AtNRAMP1 (Natural Resistance-Associated Macrophage Protein 1) in the roots and distributed within cells by AtNRAMP2 (Cailliatte et al. 2010; Alejandro et al. 2017; Gao et al. 2018). AtMTP8 (Metal Tolerance Protein 8) and AtMTP11, which belong to a different transporter family, are responsible for loading Mn from the cytosol into the vacuole or the Trans-Golgi Network (TGN), respectively (Delhaize et al. 2007; Peiter et al. 2007; Eroglu et al. 2016). The vacuole is used to store Mn excess and prevent its toxicity. However, when this element becomes scarce, other NRAMP family members, namely AtNRAMP3 and AtNRAMP4, allow the retrieval

© The Author(s) 2022. Published by Oxford University Press on behalf of Society for Molecular Biology and Evolution.

This is an Open Access article distributed under the terms of the Creative Commons Attribution License (<https://creativecommons.org/licenses/by/4.0/>), which permits unrestricted reuse, distribution, and reproduction in any medium, provided the original work is properly cited.

Open Access

of Mn from the vacuole (Lanquar et al. 2010). Mn is needed in the secretory system as a cofactor of glycosyl transferases involved in protein glycosylation (Alejandro et al. 2020). It also plays an important role as a cofactor of superoxide dismutase in mitochondria and peroxisomes (Alejandro et al. 2020). Moreover, Mn is essential for oxygenic photosynthesis as a component of the Mn_4CaO_5 cofactor of the water-splitting complex, which is bound to photosystem II (PS II) at the inner side of the thylakoid membranes (Shen 2015). CMT1 (Chloroplast Manganese Transporter 1) and PAM71 (Photosynthesis-affected mutant 71), two transporters belonging to the GDT1 family, have been shown to allow the import of Mn across the inner membrane of the chloroplast envelope and the thylakoid membrane, respectively (Schneider et al. 2016; Eisenhut et al. 2018; Zhang et al. 2018). Recently, another member of the GDT1/UPF0016 family was shown to play a crucial role in loading Mn in the Golgi apparatus, where it is needed as a cofactor of glycosyl transferases involved in cell wall formation (Yang et al. 2021). The networks of transporters that mediate uptake, storage, and distribution of other essential metals, such as Fe, Zn, and Cu, have also been described. Interestingly, these networks are interconnected, as some transporters, as well as ligands, are able to transport a broad range of metal cations (Pottier, Oomen, et al. 2015a; Seregin and Kozhevnikov 2021).

This is well illustrated when looking at the functions of transporters of the NRAMP family. This family was first identified in the context of resistance to intracellular pathogens, such *Mycobacterium tuberculosis*, in mammals. Murine NRAMP1 was shown to limit the growth of intracellular pathogens by depleting essential metals from the phagosomes where they reside (Vidal et al. 1993; Wessling-Resnick 2015). Mammalian NRAMP2 plays a central role in Fe absorption in the intestine. In yeast, the NRAMP members SMF1 and SMF2 are involved in Mn absorption and distribution, similar to *A. thaliana* NRAMP1 and NRAMP2 (Portnoy et al. 2000; Cailliatte et al. 2010; Alejandro et al. 2017; Gao et al. 2018), whereas SMF3 allows the release of Fe from the vacuole, similar to *A. thaliana* NRAMP3 and NRAMP4 (Portnoy et al. 2000; Lanquar et al. 2005). In *A. thaliana*, NRAMP1 does not only allow high-affinity Mn uptake but also plays a role in low-affinity Fe uptake (Castaings et al. 2016), clearly illustrating that these transporters connect Fe and Mn homeostasis.

While many studies have addressed the molecular mechanisms of metal homeostasis in *A. thaliana* and rice, there are only a limited number of reports on this topic in poplar. Poplars are both model trees for which the genome of several species has been sequenced (Tuskan et al. 2006; Lin et al. 2018; Zhang et al. 2019), and an industrially important crop for wood production. Poplars display outstanding growth yield among tree species and their wood is mostly used by the peeling industry to produce light packaging and plywood. Moreover, poplars are often used in the rehabilitation of polluted areas because they are highly tolerant to heavy metals and other pollutants

(Krämer 2005a; Pottier, García de la Torre, et al. 2015b). Poplar MTP family members have been functionally investigated. In the first-sequenced poplar species *Populus trichocarpa* (Tuskan et al. 2006), it has been shown that PotriMTP1 and PotriMTP11 could be the functional homologs of AtMTP1 and AtMTP11 and are involved in Zn loading into the vacuole and Mn loading into the TGN, respectively (Blaudez et al. 2003; Krämer 2005b; Peiter et al. 2007). Copper homeostasis has also been investigated in the context of photosynthetic efficiency (Ravet et al. 2011). In addition, overexpression of genes involved in Zn and Cd chelation and homeostasis has been undertaken in an attempt to increase tolerance and accumulation of these metals (Adams et al. 2011; He et al. 2015; Wang et al. 2019). Several studies have mined poplar genomic data and established lists of metal transport proteins in this species, analyzed the expression pattern of the corresponding genes and sometimes demonstrated the transport function using yeast complementation (Migeon et al. 2010; Li et al. 2015; Gao et al. 2020). These studies have often highlighted the presence of duplication in metal homeostasis genes, which is a prevalent feature in poplar genome (Tuskan et al. 2006). However, they have not investigated in detail the function of the duplicated copies.

Gene duplication is a key process in evolution. It occurs through two major processes: either whole genome duplication or local duplication by unequal crossover or transposition (Conant and Wolfe 2008). Gene duplication underlies several key events in evolution such as variation in gene copy number, the generation of new regulatory networks and the appearance of novel functions. After gene duplication occurs, relaxation of selective pressure opens the door to several scenarios. Most of the time, one of the copies undergoes nonfunctionalization through accumulation of deleterious mutations due to the lack of selective pressure on this copy. In other cases, having multiple copies of the same gene provides advantages and several functional identical genes are therefore actively maintained (Hanikenne et al. 2013). Often the copies can also undergo subfunctionalization: the preduplication function is maintained but partitioned between the two copies. Typically, the expression pattern of the ancestral gene is covered by the two copies which are expressed in different organs and involved in distinct regulatory networks (Tuskan et al. 2006). Finally, in rare cases, emergence of advantageous mutations on one of the copies can also confer a new function, which is commonly known as neofunctionalization (Moriyama et al. 2016).

In this study, we have investigated the function of poplar NRAMP3. We found that the poplar genome contains two paralogues of NRAMP3 in tandem. One of the paralogues has conserved the original function in release of metals stored in the vacuole characterized in *A. thaliana*, whereas the other paralogue has acquired a distinct localization to the TGN. Analysis of the function of this gene in transgenic poplars suggests that it has a novel function in the control of cell-to-cell transport of Mn. Therefore, the functional analysis of the two paralogues of

PotriNRAMP3 provides a clear case of neofunctionalization through change in the subcellular localization of a transporter and evidence for the involvement of the secretory pathway in cell-to-cell transport of Mn.

Results

PotriNRAMP3.1 and *PotriNRAMP3.2* are a Tandem Gene Pair Encoding Homologous Proteins

The 11 NRAMPs retrieved from *P. trichocarpa* genome V4.1 distribute into the three different phylogenetic groups of plant NRAMPs defined according to their protein sequence identities and exon-intron structures (Migeon et al. 2010, [supplementary table S1 and fig. S1A, Supplementary Material](#) online). *PotriNRAMP1*, *PotriNRAMP6.1*, and *PotriNRAMP6.2* as well as *PotriNRAMP7.1*, *PotriNRAMP7.2*, and *PotriNRAMP7.3* belong to Group I, which also includes *AtNRAMP1* and *AtNRAMP6*. *PotriNRAMP2*, *PotriNRAMP3.1*, and *PotriNRAMP3.2* are in Group II, which includes *AtNRAMP2*, *AtNRAMP5*, *AtNRAMP3*, and *AtNRAMP4*. *PotriEIN2.1* and *PotriEIN2.2* are located in the Group III as *AtEIN2* ([supplementary fig. S1A, Supplementary Material](#) online).

Interestingly, *PotriNRAMP3.1* and *PotriNRAMP3.2* genes are localized in close vicinity in *P. trichocarpa* genome. They are positioned in a 32 kb area of chromosome 7 and encode 88.2% identical proteins ([supplementary fig. S1B-C, Supplementary Material](#) online). Dot-plot analyses performed on genomic DNA including *PotriNRAMP3.1* and *PotriNRAMP3.2* genes show sequence conservation specifically between NRAMP3 loci, more precisely between their coding sequences and their 3' untranslated region, while no conservation is observed between introns ([supplementary fig. S1C-D, Supplementary Material](#) online).

NRAMP3.1 and NRAMP3.2 are Present in All Sequenced Poplar Species but not in Closely Related Species

To determine how widespread the duplication of NRAMP3 observed in *P. trichocarpa* genome is, sequences similar to *PotriNRAMP3.1* and *PotriNRAMP3.2* were retrieved using reciprocal BLASTs in nine genomes and four transcriptomes of *Populus* species, covering the five main *Populus* sections, i.e., Tacahamaca, *Populus*, *Leucoïdes*, *Turanga*, *Aigeiros*, and *Abaso* (Zhang et al. 2019; Wang et al. 2020). We could unequivocally identify two distinct sequences similar to *PotriNRAMP3.1* or *PotriNRAMP3.2*, in all investigated *Populus* genomes, i.e., *P. alba*, *P. cathayana*, *P. simonii*, *P. lasiocarpa*, *P. maximowiczii*, *P. euphratica*, *P. ussuriensis*, *P. nigra*, *P. deltoides*, *P. tremula*, *P. tremuloides*, and *P. grandidentata* ([supplementary table S1 and data S1, Supplementary Material](#) online) (Zhang et al. 2019). Evidence for two distinct sequences similar to *PotriNRAMP3.1* or *PotriNRAMP3.2* was also observed in *P. mexicana*, the single living species of the

ancestral poplar section *Abaso*, even though its genome is not fully sequenced yet ([supplementary table S1 and data S2, Supplementary Material](#) online; Wang et al. 2020). This result suggests that distinct *PotriNRAMP3.1* and *PotriNRAMP3.2* homologs are present in all *Populus* species. In contrast, blasting *PotriNRAMP3.1* and *PotriNRAMP3.2* on the genomes of three *Salix* species (*S. purpurea*, *S. suchowensis*, and *S. brachista*) and on the transcriptomes of five other *Salix* species (*S. viminalis*, *S. sachalinensis*, *S. eriocephala*, *S. fargesii*, and *S. dasyclados*) that belong to the closest phylogenetic group to *Populus* genus (Chen et al. 2019) identified a single NRAMP3 sequence in each species ([supplementary table S1 and data S1, Supplementary Material](#) online). The reciprocal BLASTs performed on *P. trichocarpa* genome provided *PotriNRAMP3.2* as best hit. These results suggest that the duplication that gave rise to NRAMP3.1 and NRAMP3.2 genes coincided with the divergence between *Populus* and *Salix* about 52 Ma (Hou et al. 2016). However, the chromosomal rearrangements that distinguish *Populus* and *Salix* genus did not affect chromosome 7, which carries the NRAMP3 loci (Hou et al. 2016). Moreover, gene collinearity is maintained around NRAMP3 loci in *P. trichocarpa* and *S. purpurea* ([fig. 1; supplementary fig. S2, Supplementary Material](#) online). Using the corresponding protein sequences of all the *Populus* and *Salix* NRAMP3 homologs identified during this analysis ([supplementary data S3 and fig. S3, Supplementary Material](#) online), we constructed a phylogenetic tree ([fig. 2](#)). This analysis showed that *Populus* NRAMP3.1 and NRAMP3.2 form distinct phylogenetic groups ([fig. 2](#)). The *Salix* homologs clearly cluster together with *Populus* NRAMP3.2 indicating that it corresponds to the ancestral copy, whereas *Populus* NRAMP3.1 sequence diverged.

To further analyze the evolutionary history of *Populus* NRAMP3.1 and NRAMP3.2 sequences, we calculated the ratio of non-synonymous (dN) versus synonymous codons (dS), between all NRAMP3.1s, between all NRAMP3.2s, and between all NRAMP3.1s and NRAMP3.2s together. Low global dN/dS around 0.2 were obtained for NRAMP3.1 and NRAMP3.2 indicating that both genes are under purifying selection. A sliding window analysis revealed that the low global dN/dS values obtained among NRAMP3.1 or NRAMP3.2 sequences result from homogeneously low ratio values along their open reading frames ([supplementary fig. S4, Supplementary Material](#) online). In contrast, comparing NRAMP3.1s with NRAMP3.2s revealed heterogeneous values along the open reading frame, with ratios above or close to 1 in the N and C termini, as expected from divergent sequences. These results suggest that sequence divergence between the two copies was driven by relaxed purifying selection, positive selection or a combination of the two, while each copy is now subject to purifying selection. The Fixed Effects Likelihood (FEL) method was then employed to investigate site-specific selective pressures specifically applied to either NRAMP3.1s or NRAMP3.2s. In this way, 21 and 4 residues under purifying selection ($P < 0.05$) were identified in NRAMP3.1s and

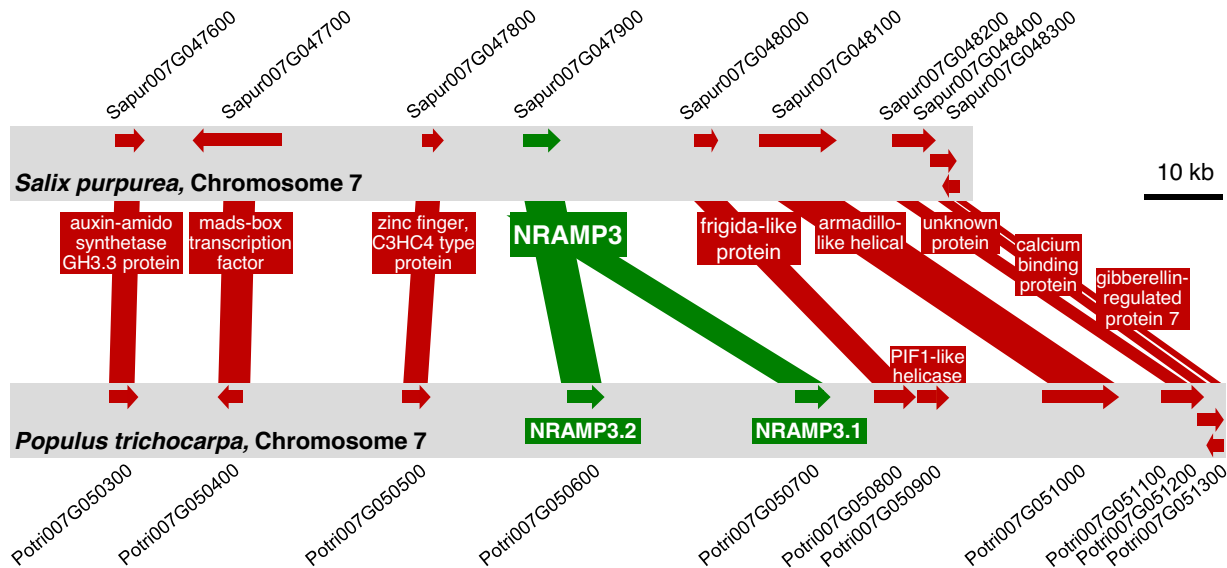


Fig. 1. Gene collinearity between *Salix purpurea* and *Populus trichocarpa* genomes is maintained in the area surrounding NRAMP3 locus which is specifically duplicated in poplars. Schematic representation of the genomic sequence around NRAMP3 loci in *P. trichocarpa* and *S. purpurea*. Gene collinearity and poplar-specific NRAMP3 duplication are supported by dot-plots analysis performed with *S. purpurea* and *P. trichocarpa* genomic sequences surrounding NRAMP3 loci (supplementary fig. S2, Supplementary Material online).

NRAMP3.2s, respectively (supplementary tables S2 and S3, Supplementary Material online). These residues are highlighted on an alignment between the consensus sequence of *Populus* NRAMP3.1 and that of *Populus* NRAMP3.2 generated from all the *Populus* NRAMP3.1 and NRAMP3.2 sequences retrieved in this study (fig. 3; supplementary data S3 and fig. S3, Supplementary Material online). Note that the four residues under purifying selection in NRAMP3.2s are also under purifying selection in NRAMP3.1s. Moreover, with the exception of V491, amino acids under purifying selection in NRAMP3.1s are conserved in NRAMP3.2s. These results suggest essential roles of these residues in the basal NRAMP3 function, common to both NRAMP3.1 and NRAMP3.2. In contrast, distinct residues were found to be under positive selection in both NRAMP3.1 (positions 3 and 437, $P < 0.05$) and NRAMP3.2 (positions 161 and 265, $P < 0.05$) (fig. 3; supplementary tables S2 and fig. S3, Supplementary Material online). These analyses indicate that NRAMP3.1 and NRAMP3.2 are not under nonfunctionalization; both sequences continue to diversify, even though they are globally under strong purifying selection. Moreover, transcript level analysis showed that NRAMP3.1 and NRAMP3.2 are both expressed in roots, stems, buds, and leaves, arguing against subfunctionalization by partitioning their expression in distinct organs of poplar (supplementary fig. S5, Supplementary Material online).

Both PotriNRAMP3.1 and PotriNRAMP3.2 Encode Functional Metal Transporters

To examine the functions of the two paralogues, we cloned *P. trichocarpa* NRAMP3.1 and NRAMP3.2 cDNAs and expressed them in yeast. Because several plant NRAMPs

were previously shown to function in Mn homeostasis, we investigated PotriNRAMP3s ability to transport this metal. For this purpose, we tested whether they could complement the *smf1* and *smf2* Mn transporter yeast mutants, which are unable to grow on low Mn condition (Cohen et al. 2000). AtNRAMP1 and AtNRAMP2, which are the functional homologs of Smf1p and Smf2p, respectively, were used as positive controls (Supek et al. 1996; Luk and Culotta 2001; Cailliatte et al. 2010; Alejandro et al. 2017). The β -glucuronidase enzyme (GUS) that has no transport activity was used as a negative control. We found that the expression of PotriNRAMP3.2 restored *smf1* growth on low Mn condition to the same extent as AtNRAMP1 (Thomine et al. 2000), whereas the expression of PotriNRAMP3.1 allowed only a partial complementation (fig. 4A). In contrast, the expression of PotriNRAMP3.1, PotriNRAMP3.2 or AtNRAMP2 fully complemented *smf2* growth defect in this condition (fig. 4B). We then took advantage of the low Mn concentration in *smf2* mutant cells to investigate the effect of PotriNRAMP3.1 and PotriNRAMP3.2 expression on Mn accumulation. We used AtNRAMP4 as a positive control, as expression of this homolog of PotriNRAMP3s was previously shown to enhance Mn accumulation in yeast (Pottier, Oomen, et al. 2015). We found that expression of PotriNRAMP3.1, PotriNRAMP3.2, or AtNRAMP4 significantly increased Mn concentration in the yeast mutant (supplementary fig. S6, Supplementary Material online). Mn concentration was 14 and 8 times higher in PotriNRAMP3.1 and PotriNRAMP3.2 expressing *smf2* strains than in *smf2* GUS control (supplementary fig. S6, Supplementary Material online). Thus, both copies of PotriNRAMP3 have retained metal transport ability. However, differences in complementation efficiency and metal accumulation suggest

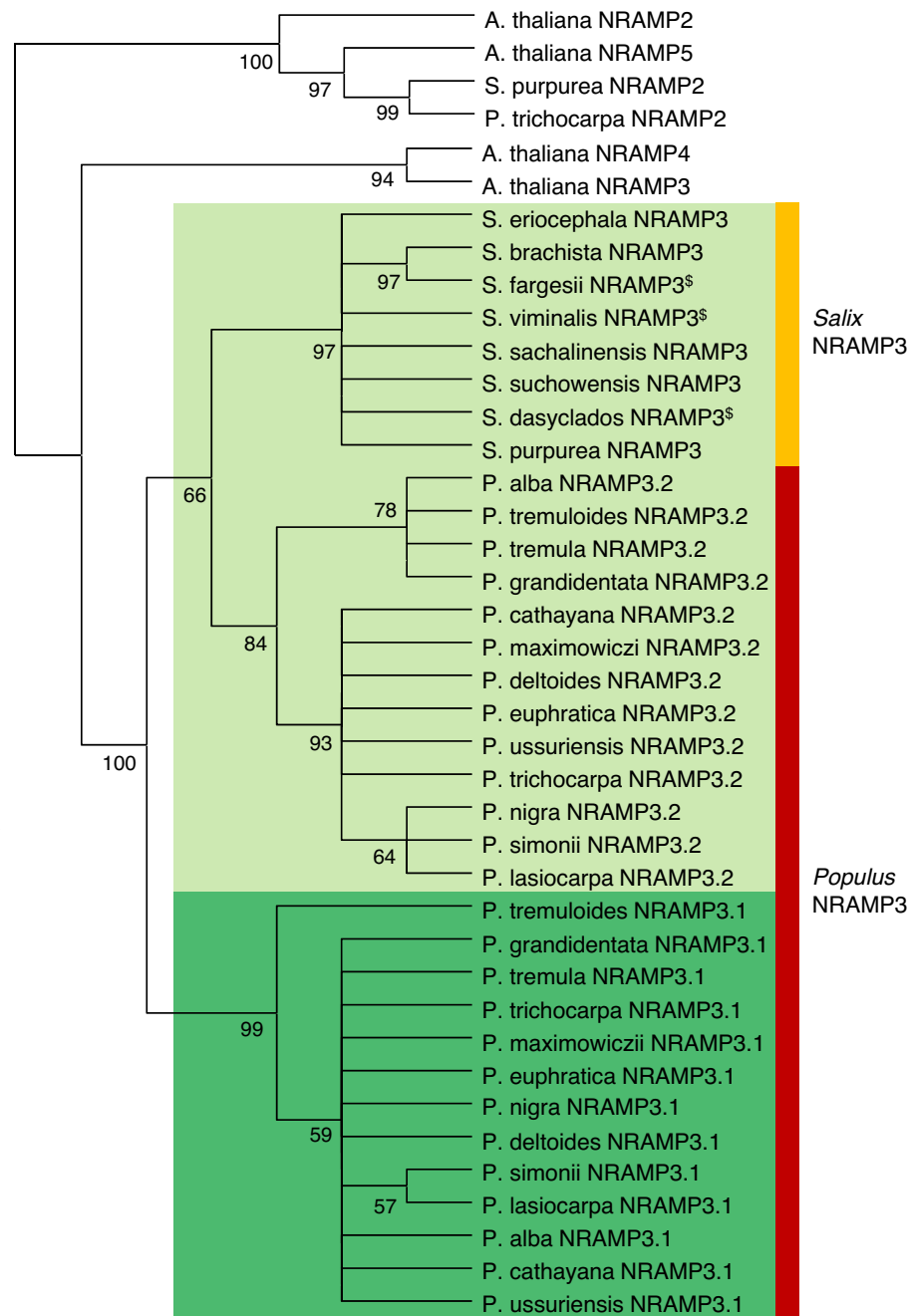


Fig. 2. Phylogenetic tree of NRAMP3 homologues in *Populus* and *Salix* species. *Arabidopsis thaliana* NRAMP2 (AT1G47240.1), NRAMP3 (AT2G23150.1), NRAMP4 (AT5G67330.1), and NRAMP5 (AT4G18790.1) as well as *P. trichocarpa* NRAMP2 (Potri002G121000.1) and *S. purpurea* NRAMP2 (Sapur.002G098200.1) are shown as an outgroup. The other protein sequences used for this tree are listed in [supplementary data S3, Supplementary Material](#) online. “§” indicates incomplete protein sequences. Phylogenetic analyses were conducted as described in Materials and methods.

differences in transport capacity or localization between these two transporters. Besides, complementation assays of the *fet3fet4* yeast strain deficient for both low- and high-affinity Fe uptake systems indicated that PotriNRAMP3.1 and PotriNRAMP3.2 are able to transport Fe in addition to Mn ([supplementary fig. S7, Supplementary Material](#) online), as previously shown for AtNRAMP3 and AtNRAMP4 ([Thomine et al. 2000](#)).

PotriNRAMP3.2, but not PotriNRAMP3.1, complements the *nramp3nramp4* double mutant of *A. thaliana*

Because both PotriNRAMP3s share high protein sequence identity with AtNRAMP3 and AtNRAMP4, we tested

whether they could perform the same function *in planta*. AtNRAMP3 and AtNRAMP4 have redundant functions in Fe remobilization from vacuoles during seed germination. As a consequence, *A. thaliana nramp3nramp4* double mutants are sensitive to Fe starvation during their early development ([Lanquar et al. 2005](#)). We expressed *PotriNRAMP3.1* and *PotriNRAMP3.2* under the *Ubiquitin 10 (pUb10)* promoter in the *A. thaliana* Columbia 0 (Col-0) *nramp3nramp4* mutant background ([Grefen et al. 2010; Bastow et al. 2018](#)), and selected three independent homozygous T3 lines expressing transgenes at various levels for further experiments ([supplementary fig. S8, Supplementary Material](#) online). Lines transformed with *pUb10:PotriNRAMP3.2* exhibited full complementation of

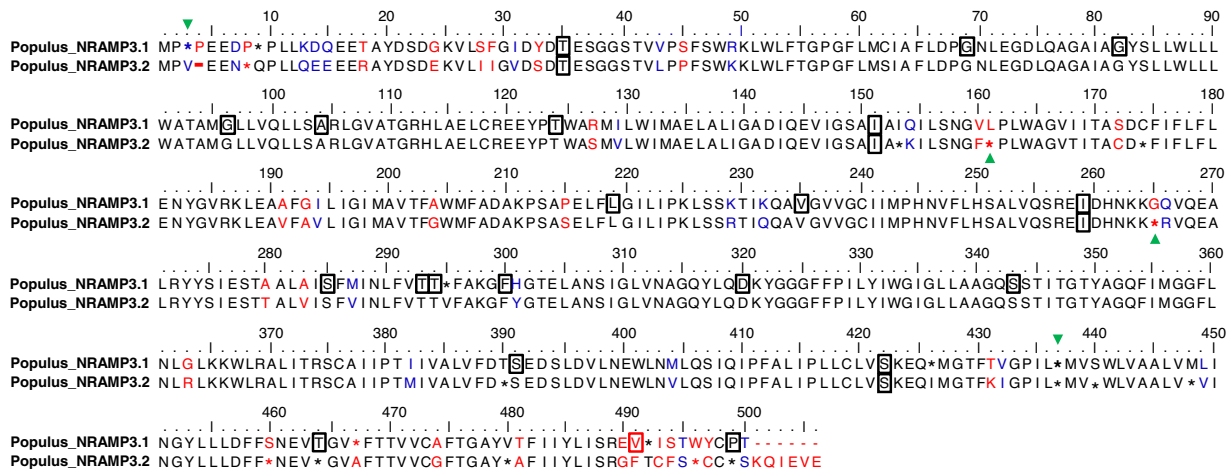


Fig. 3. Alignment of the consensus sequences of *Populus* NRAMP3.1 and NRAMP3.2. The consensus sequences were determined from the NRAMP alignments shown in [supplementary figure S3, Supplementary Material](#) online. Asterisk indicates less than 90% of conservation within *Populus* NRAMP3.1 or NRAMP3.2 cluster. Identical, similar, and different residues between the two consensus sequences are indicated in black, blue, and red, respectively. Frames indicate residues under purifying selection and green arrows indicate positive selection in either *Populus* NRAMP3.1 or NRAMP3.2 cluster according to the FEL method ($P < 0.05$). Note that NRAMP3.1 sequences contain an insertion of residue at position 4, leading to a gap (-) in NRAMP3.2 sequences.

the double mutant phenotype on Fe deficient medium: root length and cotyledon greening were indistinguishable from wild-type ([fig. 5](#)). Complementation was observed irrespective of the expression level of the transgene, indicating that even low levels are sufficient to restore the wild-type phenotype. In contrast, the expression of *PotriNRAMP3.1* did not improve the growth of the *A. thaliana nramp3nramp4* double mutant under Fe deficient

conditions, even in lines showing high expression of the transgene ([fig. 5, supplementary fig. S8, Supplementary Material](#) online). Similar results were obtained when expressing *PotriNRAMP3.1-GFP* and *PotriNRAMP3.2-GFP* under the CaMV 35S promoter (*p35S*) to study their subcellular localization in *A. thaliana* and poplar (see below), except that *p35S:PotriNRAMP3.1-GFP* partially improved *nramp3nramp4* growth under Fe deficiency

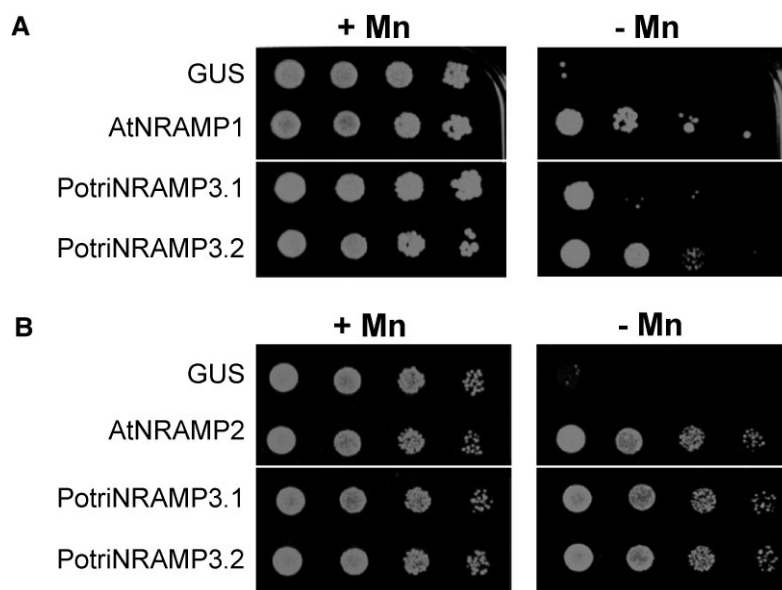


Fig. 4. *PotriNRAMP3.1* and *PotriNRAMP3.2* encode functional Mn transporters. Functional complementation of *smf1* (A) and *smf2* (B) yeast mutants. Yeast cells expressing *GUS* (negative control), *AtNRAMP1* (positive control), *AtNRAMP2* (positive control), *PotriNRAMP3.1*, or *PotriNRAMP3.2* were grown overnight. The cultures were diluted to ODs of $1-10^{-3}$ and spotted on synthetic dextrose -ura plates. Transformed *smf1* (A) strains were grown on medium supplemented with 5 mM EGTA and 100 μ M $MnSO_4$ (+Mn) or with 5 mM EGTA without $MnSO_4$ (-Mn). Transformed *smf2* (B) strains were grown in medium supplemented with 10 mM EGTA and 100 μ M $MnSO_4$ (+Mn) or with 10 mM EGTA without $MnSO_4$ (-Mn). The plates were incubated at 30°C for 5 days (*smf1*) or 2 days (*smf2*) before photography. White lines indicate cropping.

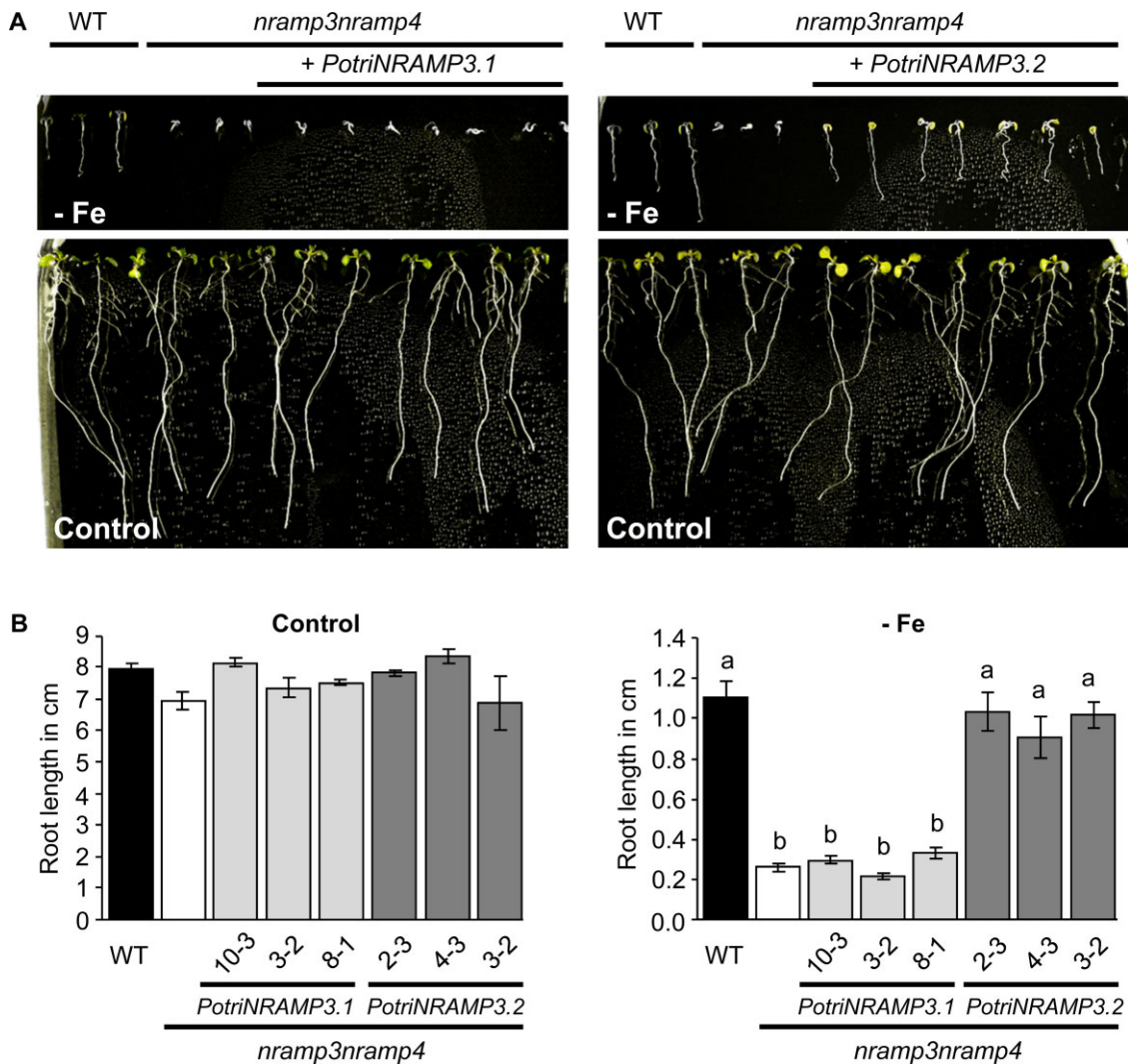


Fig. 5. *PotriNRAMP3.2* but not *PotriNRAMP3.1* expression complements the *Arabidopsis nramp3nramp4* double mutant growth defects under iron starvation. (A) Representative pictures of *nramp3nramp4 pUb10:PotriNRAMP3.1* and *pUb10:PotriNRAMP3.2* T3 *Arabidopsis* lines together with wild-type (Col-0) as positive control and *nramp3nramp4* as negative control grown vertically for 8 days in ABIS supplemented with 50 μ M FeHBED (control, bottom panel) or without iron (-Fe, top panel). (B) Quantification of main root lengths of wild-type (Col-0), *nramp3nramp4* and 3 independent *nramp3nramp4 pUb10:PotriNRAMP3.1* and *pUb10:PotriNRAMP3.2* T3 lines. Values represent mean of 10–12 roots and bars represent SD. Different letters reflect significant differences according to a Kruskal–Wallis test followed by Dunn’s test for multiple comparison ($P < 0.01$). No significant differences among genotypes were detected in the presence of Fe, left panel in (B).

(supplementary fig. S9, Supplementary Material online). Even though *PotriNRAMP3.1* is able to transport Fe (supplementary fig. S7, Supplementary Material online), it is thus not able to restore Fe remobilization during seed germination.

PotriNRAMP3.1 and PotriNRAMP3.2 have Distinct Subcellular Localizations in Plant Cells

Change in intracellular localization is one of the mechanisms leading to neofunctionalization (Ren et al. 2014). To examine *PotriNRAMP3.1* and *PotriNRAMP3.2* subcellular localizations, *A. thaliana* and poplar transgenic lines expressing C-terminal GFP fusion proteins of these two transporters were generated. Previous studies showed

that tagging with GFP at the C-terminal end does not affect NRAMP targeting and function in plants (Lanquar et al. 2005; Cailliatte et al. 2010; Alejandro et al. 2017). The *A. thaliana nramp3nramp4* double mutant (Col-0) was stably transformed with *p35S:PotriNRAMP3.1-GFP* and *p35S:PotriNRAMP3.2-GFP*. Roots of these plants were then observed by confocal microscopy (fig. 6A). Interestingly, distinct subcellular localizations were observed for *PotriNRAMP3.1-GFP* and *PotriNRAMP3.2-GFP*. While *PotriNRAMP3.2-GFP* was targeted to the vacuolar membrane, as its homologs in *A. thaliana* and *Noccaea caerulescens* (Thomine et al. 2003; Lanquar et al. 2005; Oomen et al. 2009), *PotriNRAMP3.1* was localized in intracellular punctuate structures (fig. 6A). The localization of *PotriNRAMP3.2* on the vacuolar membrane is consistent

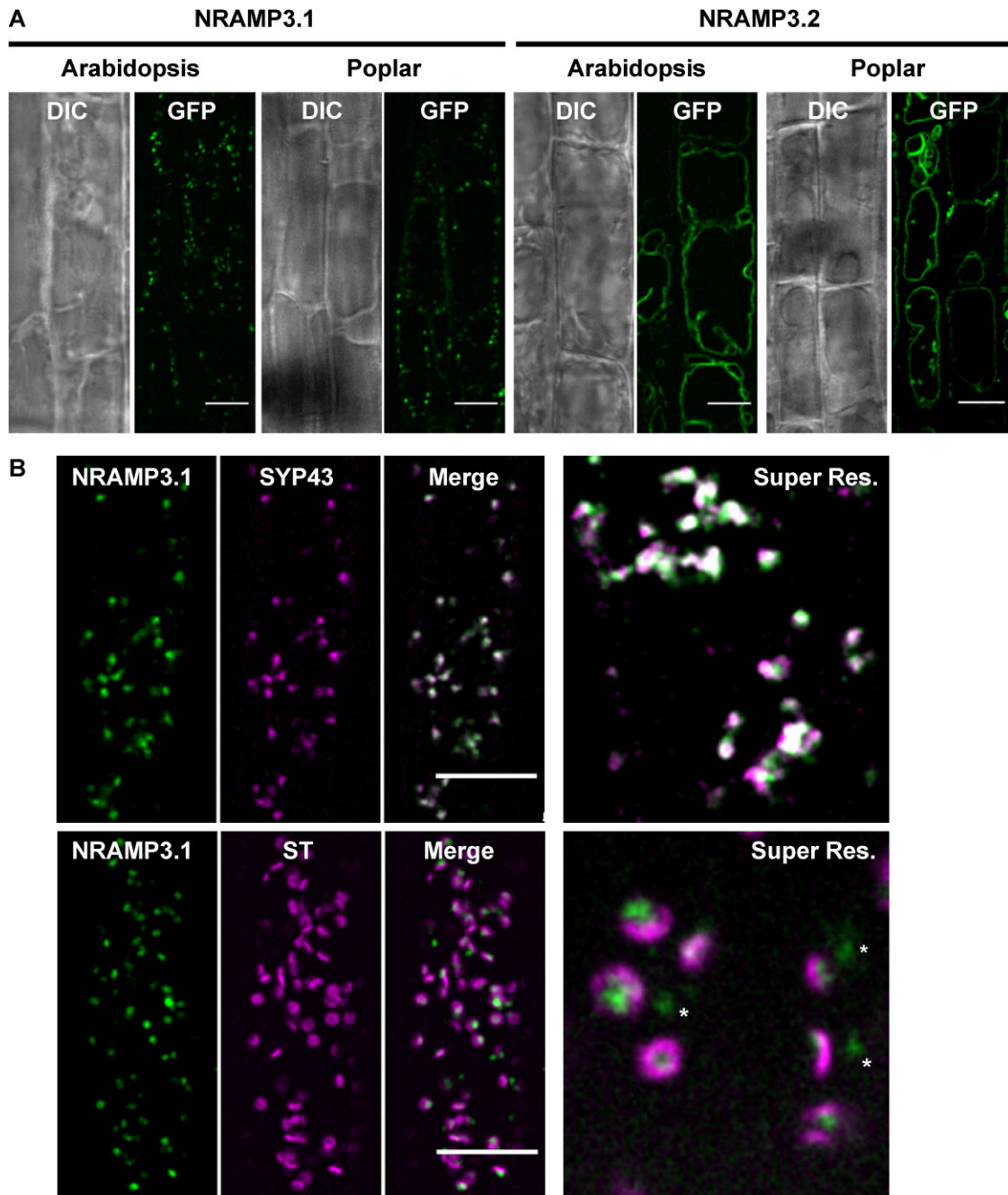


Fig. 6. PotriNRAMP3.1 localizes to the TGN while PotriNRAMP3.2 localizes to the vacuolar membrane. (A) GFP translational fusions of PotriNRAMP3.1 and PotriNRAMP3.2 were imaged in vacuolar planes by spinning disk confocal microscopy in root epidermal cells (early elongation zone) of transgenic Arabidopsis T3 seedlings and poplar. NRAMP3.1-GFP labels granular cytoplasmic structures at the cell periphery, in both Arabidopsis and Poplar. In contrast, NRAMP3.2-GFP is present on the vacuolar membrane. Transmitted-light (differential interference contrast, DIC) and fluorescence (GFP) acquisitions are shown. (B) Colocalization of PotriNRAMP3.1-GFP with the TGN marker mRFP-SYP43 (*top panel*) and juxtaposition of PotriNRAMP3.1-GFP with the trans-Golgi apparatus marker mRFP-ST (*bottom panel*) in root epidermal cells (early elongation zone) of Arabidopsis F1 seedlings. Translational fusions were imaged in the cortical planes by spinning disk confocal. Note how PotriNRAMP3.1-GFP fluorescence either faces the center of the toroidal structure of the trans-Golgi or is present as Golgi-independent structures (white asterisks). On the merged images the overlap of GFP (green) and mRFP (magenta) channels appears white. Scale bar: 10 μ m. Super resolution acquisitions (Super Res.) are 10 μ m wide.

with its ability to complement the *A. thaliana nramp3nramp4* double mutant. The partial complementation observed with PotriNRAMP3.1-GFP could be due to the mis-targeting of a small fraction of this protein, too low to generate detectable fluorescence, to the vacuolar membrane. Similar PotriNRAMP3.1 and PotriNRAMP3.2

localizations were observed in poplar root cells (fig. 6A) as well as in mesophyll protoplasts and leaf epidermal cells (supplementary fig. S10, Supplementary Material online).

To determine more precisely the subcellular localization of PotriNRAMP3.1, we tested the colocalization of PotriNRAMP3.1-GFP with RFP markers for different cell

compartments (Ebine et al. 2011; Uemura et al. 2012; Inada et al. 2016). To this aim, *A. thaliana* lines expressing PotriNRAMP3.1-GFP were crossed with stable lines expressing markers for the trans-Golgi apparatus, i.e., mRFP-ST (Sialyl Transferase), the TGN, i.e., mRFP-Syp43 and two endosomal markers, i.e., ARA6-mRFP and ARA7-mRFP. Spinning disk confocal microscopy performed on the F1 seedlings showed an extensive overlap between PotriNRAMP3.1-GFP and mRFP-SYP43 fluorescence (fig. 6B). Interestingly, although PotriNRAMP3.1-GFP fluorescence did not overlap with that of mRFP-ST, it was most often in close vicinity (fig. 6B). In contrast, little or no colocalization was observed with endosomal markers (supplementary fig. S11, Supplementary Material online). These colocalization experiments indicate that PotriNRAMP3.1 resides on the TGN, and that it is present in both Golgi-associated and Golgi-independent TGN compartments (Viotti et al. 2010; Uemura et al. 2019). Together, these results show that the *PotriNRAMP3.2* copy has retained the subcellular localization and function of the NRAMP3 genes characterized in other species, whereas *PotriNRAMP3.1* has likely acquired a novel function due to mutations that modified its subcellular localization to the TGN. However, *PotriNRAMP3.1* expression in *A. thaliana* did not lead to any phenotypic alteration that could provide hints at this novel function.

PotriNRAMP3.1, but Not PotriNRAMP3.2, Affects Manganese Homeostasis in Poplar

To investigate the functions of PotriNRAMP3.1 and PotriNRAMP3.2 in poplar, the genes coding these transporters were over-expressed as GFP fusions under the control of the *p35S*. For each construct, four independent transgenic lines over-expressing (OE) the *PotriNRAMP3s* at levels 10–25 times higher than non-transgenic (NT) control trees were analyzed (supplementary fig. S12, Supplementary Material online). Poplar lines with high levels of *PotriNRAMP3.1* expression displayed reduced height as well as internodal chlorosis on mature leaves compared with NT control trees (fig. 7A, C, F; supplementary fig. S12, Supplementary Material online). In contrast, *PotriNRAMP3.2* OE trees were indistinguishable from NT poplars (fig. 7B, C, H). To better understand the origin of the chlorosis, the maximum quantum yield of PS II was imaged using an Imaging PAM (Walz, Germany) in leaves of control poplars as well as *PotriNRAMP3.1* and *PotriNRAMP3.2* OE lines (fig. 7E, G, I). The chlorotic areas in *PotriNRAMP3.1* OE lines coincided with strongly decreased PS II maximum quantum yield (0.472 ± 0.035). In contrast, PS II efficiency was close to the optimal value of 0.82 in leaves from control (0.756 ± 0.002) and *PotriNRAMP3.2* OE trees (0.751 ± 0.008). As internodal chlorosis is a symptom of Fe deficiency and decrease in PS II efficiency may be a symptom of Mn deficiency (Connorton et al. 2017; Alejandro et al. 2020), we quantified metals in young, mature, and senescent leaves from the different poplar genotypes. These analyses revealed

that Mn concentrations in young and mature leaves were significantly lower in PotriNRAMP3.1 OE lines compared with the NT control or PotriNRAMP3.2 OE lines (fig. 8A–C). In contrast, no significant difference in Fe or Zn concentrations was detected among the different genotypes (supplementary fig. S13, Supplementary Material online). Interestingly, opposite to what was observed in leaves, Mn concentrations in stems of PotriNRAMP3.1 OE lines were higher than in NT control or PotriNRAMP3.2 OE lines (fig. 8D). Mn concentrations were also significantly higher in stems of PotriNRAMP3.2 OE lines compared with the NT control. The defect in Mn distribution observed in PotriNRAMP3.1 OE lines suggests that the phenotypes observed in these lines are due to a defect in Mn transfer from stems to leaves leading to limited Mn supply to leaves.

To further test this hypothesis, we analyzed Mn distribution in mature leaves from PotriNRAMP3.1 OE lines compared with the NT control. We dissected leaves into vein and lamina, and measured Mn separately (fig. 8E). In PotriNRAMP3.1 OE lines, the Mn concentration was lower in lamina compared with veins, whereas the concentrations in these two parts of the leaf were similar in NT control. Moreover, the Mn concentration in the lamina tended to be lower in PotriNRAMP3.1 OE lines than in the NT control line, while the opposite was observed in veins. The decrease in Mn concentration in the lamina of PotriNRAMP3.1 OE lines compared with the NT control was only significant for line 9, which displayed the most severe internodal chlorosis. These results confirm that over-expression of *PotriNRAMP3.1* in poplar perturbs Mn distribution between and within organs. Analysis of PotriNRAMP3.1 expression using RT-qPCR showed that this gene is expressed at similar levels in the lamina and the veins (supplementary fig. S14, Supplementary Material online). Together, the results presented indicate that PotriNRAMP3.1 expression can modulate Mn transport between organs and tissues.

To confirm that the leaf chlorosis symptoms observed in PotriNRAMP3.1 OE lines were due to Mn depletion in the lamina, we supplemented the trees with Mn. We grew tree cuttings for 4 weeks and then started watering half of them with 0.5 mM of MnSO_4 for an additional 5 weeks. We observed that chlorosis did not appear in newly formed leaves of Mn treated trees (supplementary fig. S15A, Supplementary Material online). In these leaves, Mn concentrations were higher in lamina and veins, but the treatment did not restore the defect in Mn distribution between these tissues (supplementary fig. S15B, Supplementary Material online). Chlorosis was not reverted in leaves formed prior to the treatment indicating that the treatment prevented chlorosis in newly formed leaves rather than corrected it in older leaves.

Discussion

In this study, we have characterized two poplar NRAMP3 metal transporters using a combination of phylogenetic,

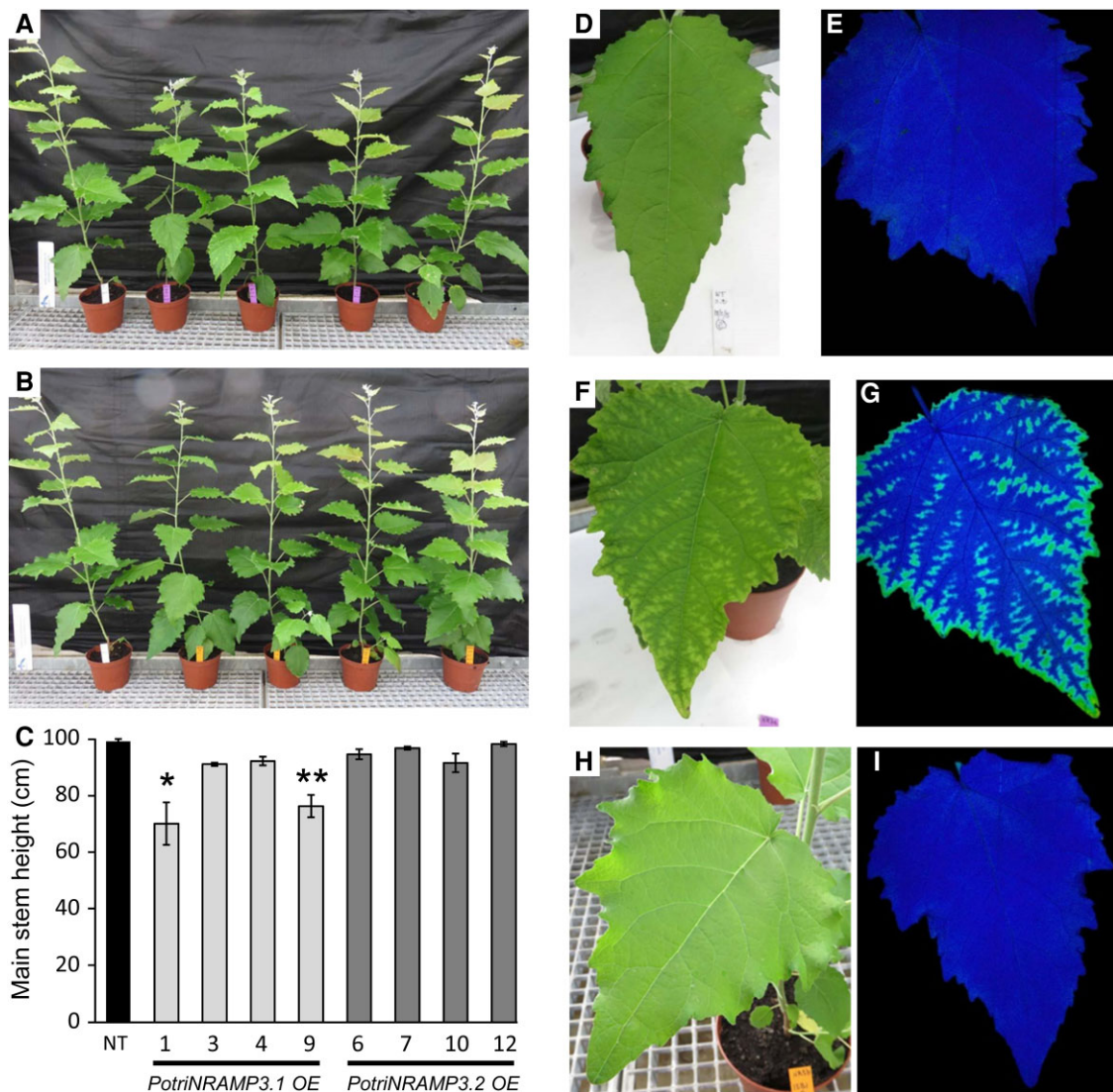


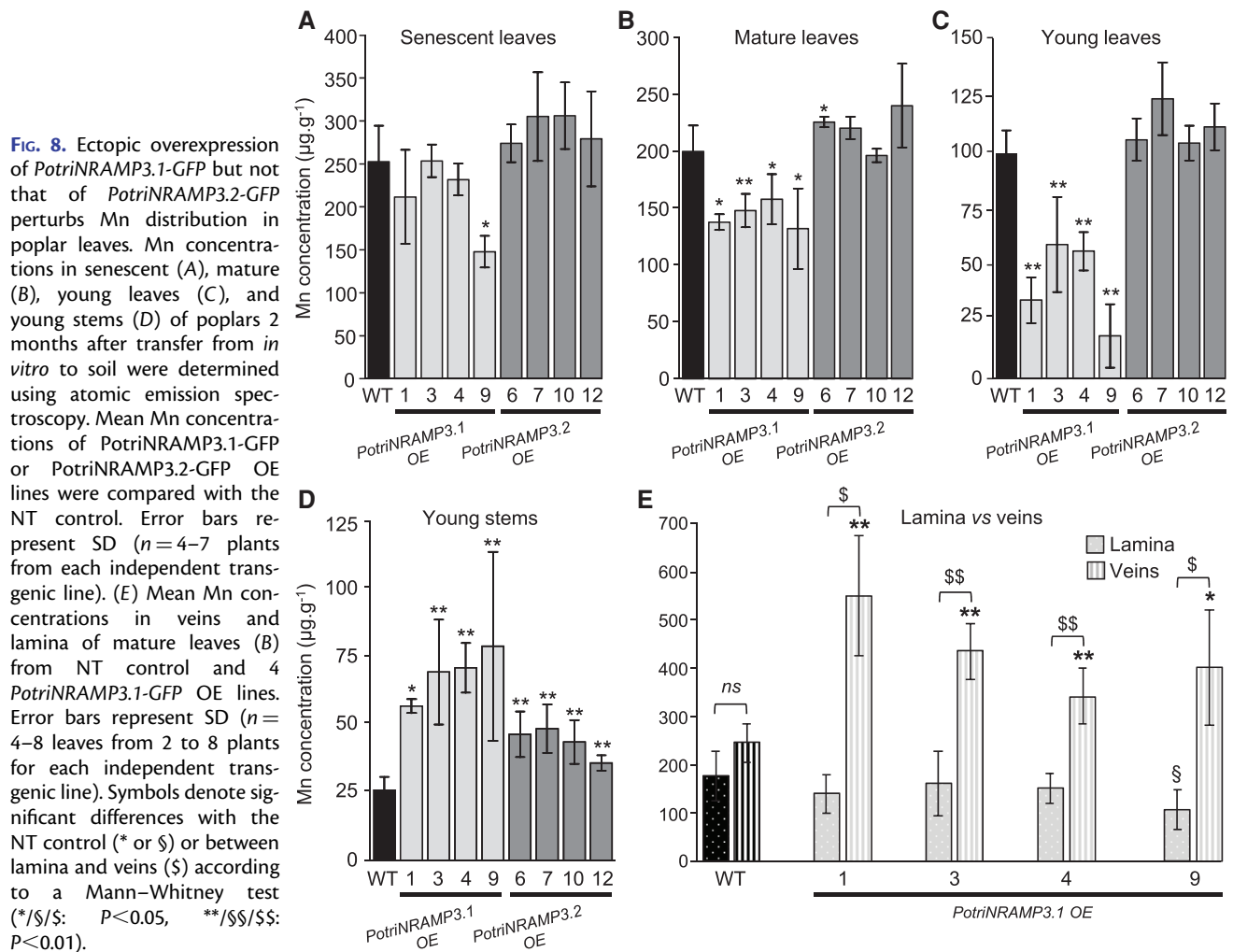
Fig. 7. The ectopic overexpression of *PotriNRAMP3.1* but not that of *PotriNRAMP3.2* leads to phenotypic alterations in poplar. Overview of four independent transgenic poplar lines OE *PotriNRAMP3.1-GFP* (A, purple tags) or *PotriNRAMP3.2-GFP* (B, orange tags) along with NT control (A and B, white tag), 2 months after transfer from *in vitro* to soil. (C) Mean heights of poplar from the different genotypes. Error bars represent SE ($n = 4-7$ trees per genotype). Asterisks denote significant difference with respect to NT control according to a Mann-Whitney test ($*P < 0.05$, $**P < 0.01$). (D-I) Leaf phenotypes of representative trees. (D, E) NT control, (F, G) *PotriNRAMP3.1-GFP* line 9 (H, I), *PotriNRAMP3.2-GFP* line 12. (D, F, H) pictures; (E, G, I) PS II maximum quantum yield measured with imaging Pulse-Amplitude-Modulation. The dark tone indicates values of F_v/F_m around 0.75 close to the optimal value of 0.8, lighter tones indicate a lower value around 0.45. Relative *PotriNRAMP3.1* and *PotriNRAMP3.2* mRNA levels of OE lines are shown in [supplementary figure S5, Supplementary Material](#) online.

cell biology and molecular genetic approaches. We found that poplar genomes harbor two tandem copies of *NRAMP3* gene under selection, whereas only one copy is present in the closest genus, *Salix*. Moreover, we demonstrated that the two paralogues encode functional metal transporters but that their functions *in planta* have diverged. Whereas *PotriNRAMP3.2* has the same function in metal retrieval from the vacuole as *AtNRAMP3* and *AtNRAMP4*, *PotriNRAMP3.1* displays a distinct subcellular localization to the TGN as well as a distinct function. Our results suggest that *PotriNRAMP3.1* could be involved in Mn distribution in poplar aerial organs. Elemental analyses show that poplar lines ectopically expressing *PotriNRAMP3.1* are impaired in Mn transfer from the

stem to the leaves and, within the leaves, from the veins to the lamina, resulting in chlorosis and a decreased PS II efficiency. Together our results show that a gene duplication of *NRAMP3* specific to the poplar genus gave rise to the neofunctionalization of one of the copies, while the other retained the conserved function described in other species and highlight an unsuspected role of the secretory pathway in cell-to-cell transport of Mn.

Distinct Mechanisms for the Formation of *NRAMP* Gene Pairs in *A. thaliana* and Poplar

Duplication events are a driving force in evolution, facilitating adaptation to changing environments. Although



gene duplication may be followed by accumulation of deleterious mutations and gene elimination, it may also lead to diversification of gene function and sub- or neofunctionalization (Yang et al. 2006). The ancestral angiosperm genome contained only 14,000 genes or less (Proost et al. 2011). However, whole genome triplications that occurred about 120 Ma significantly increased the size of the Eudicotyledon genomes.

In *A. thaliana* *AtNRAMP3* and *AtNRAMP4* encode functionally redundant metal transporters (Lanquar et al. 2005). This pair of genes located on two different chromosomes is present in *A. thaliana*, *Arabidopsis lyrata* and *N. caerulea* (Oomen et al. 2009), but only one gene is found in *Carica papaya* and *Ricinus communis* genomes. Thus, they probably originate from a duplication that took place after the *C. papaya* divergence that happened 72 Ma. The analysis of the duplicated regions of the *A. thaliana* genome showed that *AtNRAMP3* and *AtNRAMP4* loci are located on the duplicated block 0204146800380, suggesting that the pair originates from one of the two whole genome duplications that occurred between 70 and 23 Ma in the *A. thaliana* lineage (Lanquar et al. 2005; Ming et al. 2008; Proost et al. 2011).

The poplar lineage has also undergone one whole genome duplication 60–65 Ma, i.e., before the *Populus* and *Salix* divergence that took place 52 Ma (Tuskan et al. 2006; Hou et al. 2016). Comparing gene order in *S. purpurea* and in *P. trichocarpa* showed genomic collinearity upstream and downstream *NRAMP3* loci, except that only one copy of *NRAMP3* is found in *S. purpurea* (fig. 1; supplementary fig. S2, Supplementary Material online). In contrast, two copies of *NRAMP3* were found in all sequenced poplar genotypes (fig. 2). It is unlikely that the whole genome duplication accounts for the emergence of *NRAMP3.1* and *NRAMP3.2* genes specific to *Populus* species since this event happened before the *Populus* and *Salix* divergence. Moreover, gene tandem arrangements generally imply local duplication processes rather than whole genome duplications. The genomic sequence surrounding *Populus NRAMP3.1* and *NRAMP3.2* shows homologies with Class I long terminal repeats (LTR) retrotransposon elements (Gypsy) mainly located between the two genes. Retrotransposons can mediate gene duplications. However, such duplications usually create a typical intron-free copy, which can be integrated throughout the genome and not specifically close to the initial copy

(Freeling 2009). The conservation of intron/exon structure and the tandem arrangement of *Populus NRAMP3.1* and *NRAMP3.2* suggest another mechanism. Repeated sequences of retrotransposons are known to stimulate intrachromosomal recombination events or unequal crossing over, leading to gene duplication (White et al. 1994; Flagel and Wendel 2009). The genome of poplar which contains significantly more gene tandems than that of *A. thaliana* (Proost et al. 2011), contains also three time more transposons (Ming et al. 2008). Thus, it is most likely that this mechanism accounts for the tandem duplication of *Populus NRAMP3.1* and *NRAMP3.2*. Therefore, distinct mechanisms of gene duplication led to *NRAMP* gene pair formation in poplar and *A. thaliana*.

Populus NRAMP3 Copies are Subjected to Both Positive and Purifying Selection

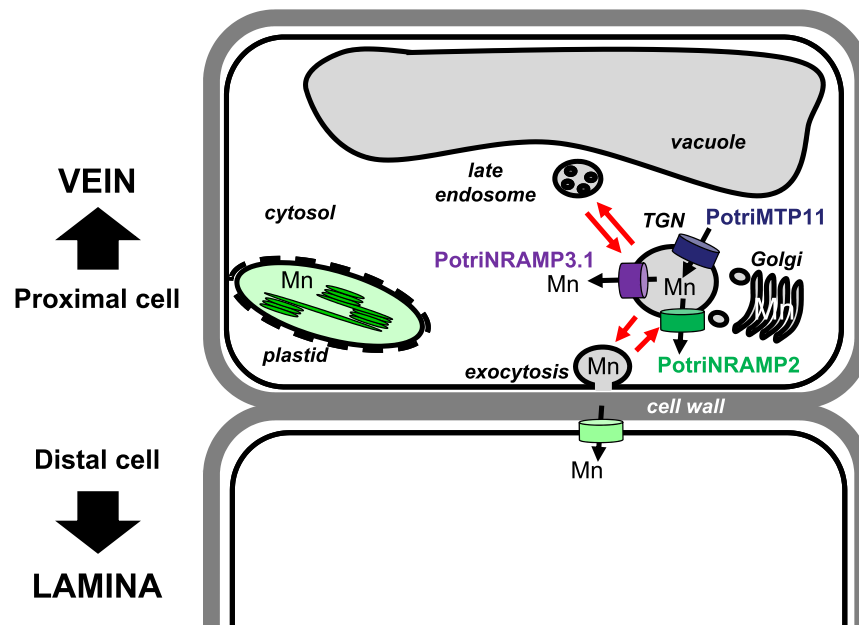
Non-synonymous (dN) versus synonymous codons (dS) analyses (dN/dS) highlight that *Populus NRAMP3.1* and *NRAMP3.2* sequences are mostly under purifying selection (fig. 3 and supplementary tables S2, S3 and fig. S3, Supplementary Material online) acting on many residues in the core conserved transmembrane domains of the protein. This is in agreement with the finding that both PotriNRAMP3.1 and PotriNRAMP3.2 have retained metal transport ability. However, the evidence suggests both positive and relaxed purifying selection especially on residues localized at the N and C terminal ends of the protein (fig. 3; supplementary tables S2, S3 and fig. S4, Supplementary Material online). Mutations in the N terminal region, where motives involved in the targeting of AtNRAMP3 and AtNRAMP4 have previously been identified, likely enabled the protein to acquire distinct subcellular localizations (Müdsam et al. 2018). The vacuolar membrane localization of PotriNRAMP3.2 (fig. 6A), its transport capacities (fig. 4; supplementary fig. S6 and S7, Supplementary Material online) and its ability to complement *A. thaliana nramp3nramp4* double mutant phenotypes (fig. 5) indicate that PotriNRAMP3.2 is the functional homolog of AtNRAMP3 and AtNRAMP4. The ability of PotriNRAMP3.1 to transport Fe and Mn in yeast (fig. 4; supplementary fig. S6 and S7, Supplementary Material online), its distinct intracellular localization (fig. 6), its inability to complement the *nramp3nramp4* double mutant phenotypes (fig. 5) and the signature of purifying selection (fig. 3, supplementary fig. S4 and tables S2, S3, Supplementary Material online) argue in favor of neofunctionalization rather than nonfunctionalization. The finding that *Populus NRAMP3.1* and *Populus NRAMP3.2* promoter sequences lack significant sequence identities further suggests that the regulation of the two copies has diverged (supplementary fig. S1D, Supplementary Material online). This is in agreement with our previous report showing that *Populus NRAMP3.1* and *NRAMP3.2* belong to different networks of coexpressed genes (Pottier, García de la Torre, et al. 2015b). We propose a scenario in which after *Populus*

NRAMP3 gene duplication, relaxation of purifying selection allowed mutations altering PotriNRAMP3.1 subcellular localization. This mutated version of *Populus NRAMP3* was subsequently maintained by purifying selection, probably because it conferred improved fitness. Specific inactivation of *Populus NRAMP3.1* would allow to further test this scenario.

PotriNRAMP3.1 Modulates Tissue Distribution of Mn

To investigate the function of PotriNRAMP3.1 and PotriNRAMP3.2 *in planta*, we generated transgenic poplars OE *PotriNRAMP3.1-GFP* and *PotriNRAMP3.2-GFP*. PotriNRAMP3.1 and PotriNRAMP3.2 subcellular localizations in poplar roots or leaves were similar to those observed in *A. thaliana*. (fig. 6; supplementary fig. S10, Supplementary Material online). Analysis of metal concentrations revealed a specific decrease in Mn concentrations in leaves from lines OE *PotriNRAMP3.1-GFP*. Moreover, lines with the lowest Mn leaf concentrations displayed internerv chlorosis (fig. 7). In agreement with the role of Mn in photosynthesis, PS II efficiency was decreased in the chlorotic parts of *PotriNRAMP3.1* OE leaves (fig. 7). Further analysis showed that the decrease in Mn leaf concentration was associated to an increase in Mn concentration in stems (fig. 8). Furthermore, Mn distribution within leaves was also affected in *PotriNRAMP3.1* OE lines: Mn accumulated at higher levels in the veins while it was depleted in the lamina. Together, these results indicate that PotriNRAMP3.1 can modulate transcellular transport of Mn. This phenotype is unexpected as PotriNRAMP3.1-GFP exhibits a clear intracellular localization to the TGN. Even though the partial complementation of *nramp3nramp4* suggests that a small fraction of PotriNRAMP3.1-GFP might be targeted to the vacuolar membrane (supplementary fig. S9, Supplementary Material online), the absence of similar phenotypes in *PotriNRAMP3.2-GFP* OE lines support the hypothesis that the fraction of PotriNRAMP3.1 associated to the TGN is responsible for the phenotypes observed in *PotriNRAMP3.1* OE lines. To account for this phenotype, we propose a working model (fig. 9) based on two hypotheses: 1) Mn cell-to-cell transport requires Mn secretion and 2) expression of *PotriNRAMP3.1* limits Mn secretion by allowing the retrieval, from the TGN of Mn, which would otherwise be secreted. PtNRAMP3.1 overexpression seems to restrict specifically Mn transfer from the veins to the lamina. However, PotriNRAMP3.1 is expressed at similar levels in the veins and in the lamina (supplementary fig. S13, Supplementary Material online). Mn secretion to the cell wall is expected to be important for cell-to-cell transfer when cells are not or poorly connected by plasmodesmata. We propose that the effect of PotriNRAMP3.1 expression is more pronounced in the lamina because 1) veins are directly supplied with Mn upon unloading from the xylem sap and 2) the density of plasmodesmata between lamina cells is lower than between the cells of the veins (Russin and Evert 1985).

Fig. 9. Working model to account of PotriNRAMP3.1 role in Mn transport from cell to cell. The model is based on the hypothesis that Mn moves through the transcellular pathway, being secreted in the apoplast via exocytosis by the cells proximal to the veins and taken up by the cells that are distal to the veins. According to this hypothesis, the transporters loading Mn (PotriMTP11) or unloading Mn (PotriNRAMP3.1 as well as PotriNRAMP2 assuming function conservation with Arabidopsis AtNRAMP2) from the secretory pathway would determine the amount of Mn made available by proximal cells for uptake by distal cells. In this context, efficient removal of Mn from the secretory pathway in the proximal cells by PotriNRAMP3.1 over-expression would limit Mn availability for the distal cell.



The function of PotriNRAMP3.1 in retrieval of Mn from the secretory system would be equivalent to the function of AtNRAMP2 (Alejandro et al. 2017; Gao et al. 2018). AtNRAMP2 localizes to the TGN and was proposed to retrieve Mn from this compartment to make it available for uptake into chloroplasts. Previous work also showed that loss of AtMTP11, which also localizes in the secretory system, leads to an increase in plant Mn concentration (Peiter et al. 2007). As AtMTP11 is involved in Mn loading into the secretory system, the observed phenotype also agrees with the hypothesis that Mn concentrations in plant tissues are, at least in part, controlled by Mn secretion. As SMF2 has also been proposed to retrieve Mn from the secretory system in yeast, the model of figure 9 would also account for the strong decrease in Mn content in the *smf2* mutant (Luk and Culotta 2001). Homologues of AtMTP11 and AtNRAMP2 are also present in poplar and could act in concert with PotriNRAMP3.1 to control the rate of Mn secretion versus intracellular distribution in poplar cells. Interestingly, mRNA levels of *PotriNRAMP2* and *PotriNRAMP3.1* are correlated in leaves (Pottier, García de la Torre, et al. 2015b).

Taken together, our results provide a clear case for neofunctionalization in a tandem of NRAMP genes specific to poplar. It also provides new insights into the cell-to-cell transport of divalent cations by showing the significant contribution of the secretory pathway in the cellular export of Mn as well as new evidence of the essential role of transporters located at the secretory pathway in the regulation of the cellular storage of Mn. In the future, it would be interesting to find out what is the advantage

conferred by the newly functionalized PotriNRAMP3.1 that led to the conservation of this gene in all examined poplar species. It will also be interesting to understand the interplay between PotriNRAMP3.1, PotriNRAMP2 and PotriMTP11 in the control of Mn concentration in the secretory pathway.

Materials and Methods

Sequences Analysis

Sequences were retrieved as indicated in [supplementary table S1, Supplementary Material](#) online. To obtain the homologous genomic sequence of *PotriNRAMP3.1* (Potri007G050600) and *PotriNRAMP3.2* (Potri007G050600) from non-assembled poplar and willow genomes, raw reads were aligned to *P. trichocarpa* genome V4.1. *PotriNRAMP3.1* and *PotriNRAMP3.2* were blasted on the obtained genome consensus using QIAGEN CLC Genomics Workbench 12.0. The best hits were then blasted back on *P. trichocarpa* genome V4.1 to confirm the sequence homology relationship. *P. trichocarpa* and *S. purpurea* genomic DNA homologies were investigated by Dot-plot analyses using Gepard softwares V1.30 and V1.40 (Krumisiek et al. 2007).

Phylogenetic Tree Construction

The tree shown in [figure 2](#) was generated from amino acid sequences listed in [supplementary data S3, Supplementary Material](#) online and outgroup sequences listed in the figure legend. For [supplementary figure S1, Supplementary Material](#) online, the accession numbers of the sequences

are provided in the figure legend. Full-length sequences were imported into the Molecular Evolutionary Genetics Analysis (MEGA) package version 7, and aligned by CLUSTALW (Kumar et al. 2016). All positions with at least 95 and 90% site coverage were used for figure 2 and supplementary figure S1, Supplementary Material online, respectively. Phylogenetic analyses were conducted using the Maximum Likelihood method. Thanks to the “Find best protein model (ML)” tool available in MEGA 7, the lower BIC (Bayesian Information Criterion) model was selected for each tree. Therefore, JTT matrix-based model and the Le_Gascuel (LG) model were used for the trees displayed in figure 2 and supplementary figure S1, Supplementary Material online, respectively (Jones et al. 1992; Le and Gascuel 2008). A discrete Gamma distribution was used to model evolutionary rate differences among sites (five categories, +G, parameter = 0.82 and parameter = 1.15 for figure 2 and supplementary fig. S1, Supplementary Material online, respectively). Initial tree(s) for the heuristic search were obtained automatically by applying Neighbor-Joining and BioNJ algorithms to a matrix of pairwise distances estimated using a JTT model, and then selecting the topology with superior log likelihood value. The bootstrap consensus tree inferred from 1,000 replicates was taken to represent the evolutionary history of the analyzed genes. Branches corresponding to partitions reproduced in less than 50% bootstrap replicates were collapsed. Trees are drawn to scale, with branch lengths measured in the number of substitutions per site. To determine the codon specific selective pressure by the FEL method (see Selective Pressure Analysis), a nucleotide substitution-based tree has also been generated. The best-fitting nucleotide model was selected by iterative procedure as described (Kosakovsky Pond and Frost 2005a), and initial estimate of the phylogeny was reconstructed by Neighbor-Joining (Saitou and Nei 1987) using the Tamura–Nei distance (Tamura and Nei 1993; Kosakovsky Pond and Frost 2005b).

Selective Pressure Analysis

After codon-based alignment, global dN/dS was first calculated for each pair of the 26 poplar NRAMP CDS using HYPHY in MEGA7. Then, the distribution of dN/dS along the protein sequence was computed through the Neij Gojobori algorithm using a 20-residue window with a shift of 10 residues using JCoDA 1.4 (Nei and Gojobori 1986; Steinway et al. 2010). Finally, positive and purifying selection at individual sites were inferred using the FEL method available at <https://www.datamonkey.org> (Kosakovsky Pond and Frost 2005b; Weaver et al. 2018). FEL generated a phylogenetic tree with the 26 Populus NRAMP CDS. A subset of branches encompassing either the NRAMP3.1 s or the NRAMP3.2 s were analyzed separately to estimate dS and dN at a site (α and β , respectively). A Maximum Likelihood approach was then undertaken to calculate the dN/dS for each codon site (ω ; $P < 0.05$).

Construction of Expression Vectors

PotriNRAMP3.1 and PotriNRAMP3.2 CDSs were amplified by PCR from cDNA synthesized from leaf RNA of *P. trichocarpa* cv Nisqually-1 using the Phusion high-fidelity DNA polymerase (Thermo-Scientific) and primers listed in supplementary table S4, Supplementary Material online. The gel-purified PCR products were recombined into pDONR207 for PotriNRAMP3.1 and into pDONR201 for PotriNRAMP3.2 following the BP Clonase (Invitrogen) manufacturer’s instruction. LR reactions were performed using the pDR195gtw vector (Rentsch et al. 1995; Oomen et al. 2009) for the generation of yeast expression vectors, and using pB7FWG2 (Karimi et al. 2002), pMDC83 (Curtis and Grossniklaus 2003) and pUB-DEST binary vectors (Grefen et al. 2010) for the generation of plant expression vectors.

Yeast Growth Assays

Yeasts were transformed as indicated in supplementary materials and methods. Transformed *smf1* and *smf2* yeast mutants were grown overnight in liquid Synthetic Dextrose -ura (SD -ura, pH 6). The cultures were diluted to ODs of $1-10^{-3}$ and spotted on SD -ura plates (pH 6). Transformed *smf1* and *smf2* strains were spotted on SD -ura, supplemented with 5 mM (*smf1*) or 10 mM (*smf2*) ethylene glycolbis (beta-aminoethyl ether)-N, N, N', N'-tetraacetic acid (EGTA) and 100 μ M MnSO₄ (+Mn) or with 5 mM (*smf1*) or 10 mM (*smf2*) EGTA without MnSO₄ (–Mn).

Confocal Imaging

Roots of *in vitro* grown 6-day-old *A. thaliana* seedlings or 2- to 3-week-old poplar explants were mounted in liquid culture medium, and confocal images of epidermal cells in the elongation zone were obtained by high-speed (100 ms) sequential acquisition of GFP ($\lambda_{ex} = 490$ nm, $\lambda_{em} = 500-550$ nm) and mRFP ($\lambda_{ex} = 590$ nm, $\lambda_{em} = 600-650$ nm), employing a Nipkow spinning disk confocal system equipped with a Prime 95Bcamera (Photometrics) and a Nikon 100 \times 1.4 aperture oil immersion objective. Super resolution images were generated with a Live-SR module for optically demodulated structured illumination (GATACA Systems). Image processing (cropping, contrast adjustment and background subtraction) was performed with ImageJ 1.45s program (Schneider et al. 2012).

Plant Material and Plant Transformation

The generation of the *nramp3nramp4* double mutants of *A. thaliana* Col-0 was described previously (Bastow et al. 2018). pUB-DEST and pB7FWG2 constructs were introduced in *nramp3nramp4* mutants through *Agrobacterium tumefaciens* (strain AGL0) mediated transformation using the flower dip method (Clough and Bent 1998). Independent homozygous *A. thaliana* Col-0 *nramp3nramp4* transformants with a single insertion locus were obtained by plant selection based on Basta resistance. The poplar INRA 717-1-B4 clone (*P. tremula* \times *P. alba*) was transformed as described in supplementary materials and

methods using media listed in [supplementary table S5, Supplementary Material](#) online (Leplé et al. 1992).

Arabidopsis thaliana Growth Conditions

A *rabidopsis thaliana* seedlings were grown on ABIS medium plates containing 2.5 mM H_3PO_4 , 5 mM KNO_3 , 2 mM $MgSO_4$, 1 mM $Ca(NO_3)_2$, MS microelements, 1% sucrose, 1% Phytigel, 1 mM MES adjusted with KOH to pH 6.1 and FeHBED (Strem Chemicals, Newburyport, MA, USA) as indicated in figure legends. FeHBED was prepared as described by Lanquar et al. (2005). For low Fe sensitivity growth assays, plants were grown for 8 days on plates where Fe was omitted. Plates were placed vertically in environmental growth chambers (Sanyo MLR-350, Morigushi, Japan) at 21°C with a 16 h photoperiod under 120 $\mu\text{mol photon m}^{-2} \text{s}^{-1}$.

PS II Maximum Quantum Yield

PS II maximum quantum yield was determined using an Imaging PAM (Walz, Germany). Efficiency of the photosynthetic electron transport (F_v/F_m) was assayed by calculating the ratio of variable fluorescence (F_v) to maximal fluorescence (F_m) after a saturating light pulse (Maxwell and Johnson 2000). Plants were dark adapted for 15 min prior to measurements. The fluorescence was measured under low measuring light (F_0) and after a flash of saturating light (F_m). F_v/F_m was calculated as $(F_m - F_0)/F_m$. Five areas of interest of each leaf were selected for quantification in three leaves from different individuals of each genotype.

Root Length Measurements

Plants grown vertically on plates were photographed at the indicated times and root length was determined using ImageJ and a digitizer tablet (Schneider et al. 2012; Intuos 4 M WACOM, Krefeld, Germany).

Elemental Analysis

For metal analyses in yeast, liquid SD -ura medium containing transformed *smf2* strain growing overnight were diluted to OD 0.3 in liquid SD -ura supplemented with 30 μM $FeCl_3$ and 10 μM $MnSO_4$. After 30 h of incubation at 30°C under agitation, yeast cells were recovered by centrifugation ($3,340 \times g$, 5 min, 4°C) and washed twice in 50 ml ice cold YNB supplemented with EDTA 20 mM and MES 50 mM pH6, pelleted and then washed in ice cold ultrapure water. For metal analyses in plants, tissues were harvested and washed. The dry weight of the samples (yeasts or plants) was measured after drying at 60°C for 3 days. Dried samples were mineralized and analyzed for metal content as previously described (Pottier et al. 2019).

Statistical Analysis

Data were analyzed with Kruskal–Wallis and Mann–Whitney non-parametric tests for multiple comparisons and pair comparisons, respectively. For multiple comparisons, a Dunn's post hoc test was performed when

significant differences were detected. Both tests were performed using GraphPad Prism 7.

Acknowledgments

This work was supported by grants from the DIM Astréa (Région Ile-de-France) to M.P., from the VIED organization to V.A.L.T., ANR PHYTOPOP (ANR-06-ECOT-0015) and MOBIFER (ANR-17-CE20-0008-02) to S.T. C.P.-B. was funded by AgriObtentions. The S.T. team is supported by the CNRS and benefits and from the support of Saclay Plant Sciences-SPS (ANR-17-EUR-0007). The present work has benefited from Imagerie-Gif core facility supported by l'Agence Nationale de la Recherche (ANR-11-EQPX-0029/Morphoscope, ANR-10-INBS-04/FranceBioImaging). The authors thank Prof. Wolf B. Frommer for providing support.

Data Availability Statement

The data underlying this article are available in the article and in its online [supplementary material](#).

Supplementary Material

[Supplementary data](#) are available at *Molecular Biology and Evolution* online.

References

- Adams JP, Adeli A, Hsu C-Y, Harkess RL, Page GP, dePamphilis CW, Schultz EB, Yuceer C. 2011. Poplar maintains zinc homeostasis with heavy metal genes HMA4 and PCS1. *J Exp Bot* **62**: 3737–3752.
- Alejandro S, Cailliatte R, Alcon C, Dirick L, Domergue F, Correia D, Castaings L, Briat J-F, Mari S, Curie C. 2017. Intracellular distribution of manganese by the *Trans*-golgi network transporter NRAMP2 is critical for photosynthesis and cellular redox homeostasis. *Plant Cell* **29**:3068–3084.
- Alejandro S, Höller S, Meier B, Peiter E. 2020. Manganese in plants: from acquisition to subcellular allocation. *Front Plant Sci* **11**:300.
- Bastow EL, de la Torre VS G, Maclean AE, Green RT, Merlot S, Thomine S, Balk J. 2018. Vacuolar iron stores gated by NRAMP3 and NRAMP4 are the primary source of iron in germinating seeds. *Plant Physiol* **177**:1267–1276.
- Blaudez D, Kohler A, Martin F, Sanders D, Chalot M. 2003. Poplar metal tolerance protein 1 confers zinc tolerance and is an oligomeric vacuolar zinc transporter with an essential leucine zipper motif. *Plant Cell* **15**:2911–2928.
- Cailliatte R, Schikora A, Briat J-F, Mari S, Curie C. 2010. High-affinity manganese uptake by the metal transporter NRAMP1 is essential for *Arabidopsis* growth in low manganese conditions. *Plant Cell* **22**:904–917.
- Castaings L, Caquot A, Loubet S, Curie C. 2016. The high-affinity metal Transporters NRAMP1 and IRT1 Team up to Take up Iron under Sufficient Metal Provision. *Sci Rep* **6**:37222.
- Chen J, Huang Y, Brachi B, Yun Q, Zhang W, Lu W, Li H, Li W, Sun X, Wang G, et al. 2019. Genome-wide analysis of Cushion willow provides insights into alpine plant divergence in a biodiversity hotspot. *Nat Commun* **10**:5230.
- Clough SJ, Bent AF. 1998. Floral dip: a simplified method for Agrobacterium-mediated transformation of *Arabidopsis thaliana*: Floral dip transformation of *Arabidopsis*. *Plant J* **16**:735–743.

- Cohen A, Nelson H, Nelson N. 2000. The family of SMF metal ion transporters in yeast cells. *J Biol Chem* **275**:33388–33394.
- Conant GC, Wolfe KH. 2008. Turning a hobby into a job: How duplicated genes find new functions. *Nat Rev Genet* **9**:938–950.
- Connorton JM, Balk J, Rodríguez-Celma J. 2017. Iron homeostasis in plants – a brief overview. *Metallomics* **9**:813–823.
- Curtis MD, Grossniklaus U. 2003. A gateway cloning vector set for high-throughput functional analysis of genes in planta. *Plant Physiol* **133**:462–469.
- Delhaize E, Gruber BD, Pittman JK, White RG, Leung H, Miao Y, Jiang L, Ryan PR, Richardson AE. 2007. A role for the *AtMTP11* gene of Arabidopsis in manganese transport and tolerance: A role for *AtMTP11* in Mn transport and tolerance. *Plant J* **51**:198–210.
- Ebine K, Fujimoto M, Okatani Y, Nishiyama T, Goh T, Ito E, Dainobu T, Nishitani A, Uemura T, Sato MH, et al. 2011. A membrane trafficking pathway regulated by the plant-specific RAB GTPase ARA6. *Nat Cell Biol* **13**:853–859.
- Eisenhut M, Hoecker N, Schmidt SB, Basgaran RM, Flachbart S, Jahns P, Eser T, Geimer S, Husted S, Weber APM, et al. 2018. The plastid envelope chloroplast manganese transporter1 is essential for manganese homeostasis in arabidopsis. *Mol Plant* **11**:955–969.
- Eroglu S, Meier B, von Wirén N, Peiter E. 2016. The vacuolar manganese transporter MTP8 determines tolerance to iron deficiency-induced chlorosis in arabidopsis. *Plant Physiol* **170**:1030–1045.
- Flagel LE, Wendel JF. 2009. Gene duplication and evolutionary novelty in plants. *New Phytol* **183**:557–564.
- Freeling M. 2009. Bias in plant gene content following different sorts of duplication: tandem, whole-genome, segmental, or by transposition. *Annu Rev Plant Biol* **60**:433–453.
- Gao H, Xie W, Yang C, Xu J, Li J, Wang H, Chen X, Huang C-F. 2018. NRAMP2, a trans-Golgi network-localized manganese transporter, is required for Arabidopsis root growth under manganese deficiency. *New Phytol* **217**:179–193.
- Gao Y, Yang F, Liu J, Xie W, Zhang L, Chen Z, Peng Z, Ou Y, Yao Y. 2020. Genome-Wide Identification of Metal Tolerance Protein Genes in Populus trichocarpa and Their Roles in Response to Various Heavy Metal Stresses. *Int J Mol Sci* **21**:1680.
- Grefen C, Donald N, Hashimoto K, Kudla J, Schumacher K, Blatt MR. 2010. A ubiquitin-10 promoter-based vector set for fluorescent protein tagging facilitates temporal stability and native protein distribution in transient and stable expression studies: Fluorescence tagging and expression in Arabidopsis. *Plant J* **64**:355–365.
- Hanikenne M, Kroymann J, Trampczynska A, Bernal M, Motte P, Clemens S, Krämer U. 2013. Hard selective sweep and ectopic gene conversion in a gene cluster affording environmental adaptation. Bomblies K, editor. *PLoS Genet* **9**:e1003707.
- He J, Li H, Ma C, Zhang Y, Polle A, Rennenberg H, Cheng X, Luo Z. 2015. Overexpression of bacterial γ -glutamylcysteine synthetase mediates changes in cadmium influx, allocation and detoxification in poplar. *New Phytol* **205**:240–254.
- Hou J, Ye N, Dong Z, Lu M, Li L, Yin T. 2016. Major chromosomal rearrangements distinguish willow and poplar after the ancestral “Salicoid” genome duplication. *Genome Biol Evol* **8**:1868–1875.
- Inada N, Betsuyaku S, Shimada TL, Ebine K, Ito E, Kutsuna N, Hasezawa S, Takano Y, Fukuda H, Nakano A, et al. 2016. Modulation of plant RAB GTPase-mediated membrane trafficking pathway at the interface between plants and obligate biotrophic pathogens. *Plant Cell Physiol* **57**:1854–1864.
- Jones DT, Taylor WR, Thornton JM. 1992. The rapid generation of mutation data matrices from protein sequences. *Bioinformatics* **8**:275–282.
- Karimi M, Inzé D, Depicker A. 2002. GATEWAY™ vectors for Agrobacterium-mediated plant transformation. *Trends Plant Sci* **7**:193–195.
- Kosakovsky Pond SL, Frost SDW. 2005a. A Simple hierarchical approach to modeling distributions of substitution rates. *Mol Biol Evol* **22**:223–234.
- Kosakovsky Pond SL, Frost SDW. 2005b. Not so different after all: a comparison of methods for detecting amino acid sites under selection. *Mol Biol Evol* **22**:1208–1222.
- Krämer U. 2005a. Phytoremediation: novel approaches to cleaning up polluted soils. *Curr Opin Biotechnol* **16**:133–141.
- Krämer U. 2005b. MTP1 mops up excess zinc in Arabidopsis cells. *Trends Plant Sci* **10**:313–315.
- Krumsiek J, Arnold R, Rattei T. 2007. Gepard: a rapid and sensitive tool for creating dotplots on genome scale. *Bioinformatics* **23**:1026–1028.
- Kumar S, Stecher G, Tamura K. 2016. MEGA7: molecular evolutionary genetics analysis version 7.0 for bigger datasets. *Mol Biol Evol* **33**:1870–1874.
- Lanquar V, Lelièvre F, Bolte S, Hamès C, Alcon C, Neumann D, Vansuyt G, Curie C, Schröder A, Krämer U, et al. 2005. Mobilization of vacuolar iron by AtNRAMP3 and AtNRAMP4 is essential for seed germination on low iron: Iron mobilization during seed germination. *EMBO J* **24**:4041–4051.
- Lanquar V, Ramos MS, Lelièvre F, Barbier-Brygoo H, Krieger-Liszskay A, Krämer U, Thomine S. 2010. Export of vacuolar manganese by AtNRAMP3 and AtNRAMP4 is required for optimal photosynthesis and growth under manganese deficiency. *Plant Physiol* **152**:1986–1999.
- Le SQ, Gascuel O. 2008. An improved general amino acid replacement matrix. *Mol Biol Evol* **25**:1307–1320.
- Lepié JC, Brasileiro AC, Michel MF, Delmotte F, Jouanin L. 1992. Transgenic poplars: expression of chimeric genes using four different constructs. *Plant Cell Rep* **11**:137–141.
- Li D, Xu X, Hu X, Liu Q, Wang Z, Zhang H, Han W, Wei M, Hanzeng W, Liu H, et al. 2015. Genome-wide analysis and heavy metal-induced expression profiling of the HMA gene family in Populus trichocarpa. *Front Plant Sci* **6**:1149.
- Lin Y-C, Wang J, Delhomme N, Schiffthaler B, Sundström G, Zuccolo A, Nystedt B, Hvidsten TR, de la Torre A, Cossu RM, et al. 2018. Functional and evolutionary genomic inferences in Populus through genome and population sequencing of American and European aspen. *Proc Natl Acad Sci U S A* **115**:E10970–E10978.
- Luk EE, Culotta VC. 2001. Manganese superoxide dismutase in Saccharomyces cerevisiae acquires its metal co-factor through a pathway involving the Nramp metal transporter, Smf2p. *J Biol Chem* **276**:47556–47562.
- Maxwell K, Johnson GN. 2000. Chlorophyll fluorescence—a practical guide. *J Exp Bot* **51**:659–668.
- Migeon A, Blaudez D, Wilkins O, Montanini B, Campbell MM, Richaud P, Thomine S, Chalot M. 2010. Genome-wide analysis of plant metal transporters, with an emphasis on poplar. *Cell Mol Life Sci* **67**:3763–3784.
- Ming R, Hou S, Feng Y, Yu Q, Dionne-Laporte A, Saw JH, Senin P, Wang W, Ly BV, Lewis KLT, et al. 2008. The draft genome of the transgenic tropical fruit tree papaya (Carica papaya Linnaeus). *Nature* **452**:991–996.
- Moriyama Y, Ito F, Takeda H, Yano T, Okabe M, Kuraku S, Keeley FW, Koshiba-Takeuchi K. 2016. Evolution of the fish heart by sub/neofunctionalization of an elastin gene. *Nat Commun* **7**:10397.
- Müdsam C, Wollschläger P, Sauer N, Schneider S. 2018. Sorting of Arabidopsis NRAMP3 and NRAMP4 depends on adaptor protein complex AP4 and a dileucine-based motif. *Traffic* **19**:503–521.
- Nei M, Gojobori T. 1986. Simple methods for estimating the numbers of synonymous and nonsynonymous nucleotide substitutions. *Mol Biol Evol* **3**:418–426.
- Oomen RJF, Wu J, Lelièvre F, Blanchet S, Richaud P, Barbier-Brygoo H, Aarts MGM, Thomine S. 2009. Functional characterization of NRAMP3 and NRAMP4 from the metal hyperaccumulator *Thlaspi caerulescens*. *New Phytol* **181**:637–650.
- Peiter E, Montanini B, Gobert A, Pedas P, Husted S, Maathuis FJM, Blaudez D, Chalot M, Sanders D. 2007. A secretory pathway-localized cation diffusion facilitator confers plant manganese tolerance. *Proc Natl Acad Sci* **104**:8532–8537.

- Portnoy ME, Liu XF, Culotta VC. 2000. *Saccharomyces cerevisiae* expresses three functionally distinct homologues of the nramp family of metal transporters. *Mol Cell Biol* **20**:7893–7902.
- Pottier M, Dumont J, Masclaux-Daubresse C, Thomine S. 2019. Autophagy is essential for optimal translocation of iron to seeds in *Arabidopsis*. *J Exp Bot* **70**:859–869.
- Pottier M, Oomen R, Picco C, Giraudat J, Scholz-Starke J, Richaud P, Carpaneto A, Thomine S. 2015a. Identification of mutations allowing Natural Resistance Associated Macrophage Proteins (NRAMP) to discriminate against cadmium. *Plant J* **83**:625–637.
- Pottier M, García de la Torre V, Victor C, David LC, Chalot M, Thomine S. 2015b. Genotypic variations in the dynamics of metal concentrations in poplar leaves: A field study with a perspective on phytoremediation. *Environ Pollut* **199**:73–82.
- Proost S, Pattyn P, Gerats T, Van de Peer Y. 2011. Journey through the past: 150 million years of plant genome evolution: One hundred and fifty million years of plant genome evolution. *Plant J* **66**:58–65.
- Ravet K, Danford FL, Dihle A, Pittarello M, Pilon M. 2011. Spatiotemporal analysis of copper homeostasis in *Populus trichocarpa* reveals an integrated molecular remodeling for a preferential allocation of copper to plastocyanin in the chloroplasts of developing leaves. *Plant Physiol* **157**:1300–1312.
- Ren L-L, Liu Y-J, Liu H-J, Qian T-T, Qi L-W, Wang X-R, Zeng Q-Y. 2014. Subcellular relocalization and positive selection play key roles in the retention of duplicate genes of *Populus* class III peroxidase family. *Plant Cell* **26**(6):2404–2419.
- Rentsch D, Laloi M, Rouhara I, Schmelzer E, Delrot S, Frommer WB. 1995. *NTR1* encodes a high affinity oligopeptide transporter in *Arabidopsis*. *FEBS Lett* **370**:264–268.
- Russin WA, Evert RF. 1985. Studies on the leaf of *Populus deltoides* (*Salicaceae*): ultrastructure, plasmodesmatal frequency and solute concentrations. *Am J Bot* **72**:1232–1247.
- Saitou N, Nei M. 1987. The neighbor-joining method: a new method for reconstructing phylogenetic trees. *Mol Biol Evol* **4**:406–425.
- Schneider CA, Rasband WS, Eliceiri KW. 2012. NIH Image to ImageJ: 25 years of image analysis. *Nat Methods* **9**:671–675.
- Schneider A, Steinberger I, Herdean A, Gandini C, Eisenhut M, Kurz S, Morper A, Hoecker N, Rühle T, Labs M, et al. 2016. The evolutionarily conserved protein PHOTOSYNTHESIS AFFECTED MUTANT71 is required for efficient manganese uptake at the thylakoid membrane in *Arabidopsis*. *Plant Cell* **28**:892–910.
- Seregin IV, Kozhevnikova AD. 2021. Low-molecular-weight ligands in plants: role in metal homeostasis and hyperaccumulation. *Photosynth Res* **150**:51–96.
- Shen J-R. 2015. The structure of photosystem II and the mechanism of water oxidation in photosynthesis. *Annu Rev Plant Biol* **66**:23–48.
- Steinway SN, Dannenfels R, Laucius CD, Hayes JE, Nayak S. 2010. JCoDA: a tool for detecting evolutionary selection. *BMC Bioinformatics* **11**:284.
- Supek F, Supekova L, Nelson H, Nelson N. 1996. A yeast manganese transporter related to the macrophage protein involved in conferring resistance to mycobacteria. *Proc Natl Acad Sci* **93**:5105–5110.
- Tamura K, Nei M. 1993. Estimation of the number of nucleotide substitutions in the control region of mitochondrial DNA in humans and chimpanzees. *Mol Biol Evol* **10**:512–526.
- Thomine S, Lelièvre F, Debarbieux E, Schroeder J-I, Barbier-Brygoo H. 2003. AtNRAMP3, a multispecific vacuolar metal transporter involved in plant responses to iron deficiency. *Plant J* **34**(5): 685–695.
- Thomine S, Wang R, Ward JM, Crawford NM, Schroeder JI. 2000. Cadmium and iron transport by members of a plant metal transporter family in *Arabidopsis* with homology to Nramp genes. *Proc Natl Acad Sci* **97**:4991–4996.
- Tuskan GA, DiFazio S, Jansson S, Bohlmann J, Grigoriev I, Hellsten U, Putnam N, Ralph S, Rombauts S, Salamov A, et al. 2006. The genome of black cottonwood, *Populus trichocarpa* (Torr. & Gray). *Science* **313**:1596–1604.
- Uemura T, Kim H, Saito C, Ebine K, Ueda T, Schulze-Lefert P, Nakano A. 2012. Qa-SNAREs localized to the trans-Golgi network regulate multiple transport pathways and extracellular disease resistance in plants. *Proc Natl Acad Sci* **109**:1784–1789.
- Uemura T, Nakano RT, Takagi J, Wang Y, Kramer K, Finkemeier I, Nakagami H, Tsuda K, Ueda T, Schulze-Lefert P, et al. 2019. A golgi-released subpopulation of the trans-golgi network mediates protein secretion in *Arabidopsis*. *Plant Physiol* **179**:519–532.
- Vidal SM, Malo D, Vogan K, Skamene E, Gros P. 1993. Natural resistance to infection with intracellular parasites: Isolation of a candidate for Bcg. *Cell* **73**:469–485.
- Viotti C, Bubeck J, Stierhof Y-D, Krebs M, Langhans M, van den Berg W, van Dongen W, Richter S, Geldner N, Takano J, et al. 2010. Endocytic and secretory traffic in *Arabidopsis* merge in the trans-golgi network/early endosome, an independent and highly dynamic organelle. *Plant Cell* **22**:1344–1357.
- Wang H, Yuanyuan L, Peng Z, Li J, Huang W, Yan L, Wang X, Xie S, Sun L, Han E, et al. 2019. Ectopic expression of poplar ABC transporter PtoABCG36 confers Cd tolerance in *Arabidopsis thaliana*. *Int J Mol Sci* **20**:3293.
- Wang M, Zhang L, Zhang Z, Li M, Wang D, Zhang X, Xi Z, Keefover-Ring K, Smart LB, DiFazio SP, et al. 2020. Phylogenomics of the genus *Populus* reveals extensive interspecific gene flow and balancing selection. *New Phytol* **225**: 1370–1382.
- Weaver S, Shank SD, Spielman SJ, Li M, Muse SV, Kosakovsky Pond SL. 2018. Datamonkey 2.0: a modern web application for characterizing selective and other evolutionary processes. *Mol Biol Evol* **35**:773–777.
- Wessling-Resnick M. 2015. Nramp1 and other transporters involved in metal withholding during infection. *J Biol Chem* **290**: 18984–18990.
- White SE, Habera LF, Wessler SR. 1994. Retrotransposons in the flanking regions of normal plant genes: a role for copia-like elements in the evolution of gene structure and expression. *Proc Natl Acad Sci* **91**:11792–11796.
- Yang X, Tuskan G A, Cheng Z M. 2006. Divergence of the Dof gene families in poplar, *Arabidopsis*, and rice suggests multiple modes of gene evolution after duplication. *Plant Physiol* **142**(3): 820–830.
- Yang C-H, Wang C, Singh S, Fan N, Liu S, Zhao L, Cao H, Xie W, Yang C, Huang C. 2021. Golgi-localised manganese transporter PML3 regulates *Arabidopsis* growth through modulating Golgi glycosylation and cell wall biosynthesis. *New Phytol.* **nph 17209**.
- Zhang B, Zhang C, Liu C, Jing Y, Wang Y, Jin L, Yang L, Fu A, Shi J, Zhao F, et al. 2018. Inner envelope CHLOROPLAST MANGANESE TRANSPORTER 1 supports manganese homeostasis and phototrophic growth in *Arabidopsis*. *Mol Plant* **11**:943–954.
- Zhang B, Zhu W, Diao S, Wu X, Lu J, Ding C, Su X. 2019. The poplar pangenome provides insights into the evolutionary history of the genus. *Commun Biol* **2**:215.